First dual AK/GSK-3β inhibitors endowed with antioxidant properties as multifunctional, potential neuroprotective agents

First Dual AK/GSK-3β Inhibitors Endowed with Antioxidant Properties as Multifunctional, Potential Neuroprotective Agents

Simone Brogi,[a,1] Anna Ramunno,[b,1] Lida Savi,[c] Giulia Chemi,[a] Gloria Alfano,[a] Alessandra Pecorelli,[d] Erika Pambianchi,[d] Paola Galatello,[b] Giulia Compagnoni,[c] Federico Focher,[c,*] Giuseppe Biamonti,[c] Giuseppe Valacchi,[d,e] Stefania Butini,[a,*] Sandra Gemma,[a,*] Giuseppe Campiani,[a] Margherita Brindisi[a]

[a]*European Research Centre for Drug Discovery and Development (NatSynDrugs) and Department of Biotechnology, Chemistry, and Pharmacy, Università degli Studi di Siena via Aldo Moro 2, 53100 Siena, Italy.*
[b]*Dipartimento di Farmacia/DIFARMA, Università degli Studi di Salerno, via Giovanni Paolo II 132, 84084 Fisciano, Salerno, Italy.*
[c]*Istituto di Genetica Molecolare, CNR, via Abbiategrasso 207, 27100 Pavia, Italy*
[d]*Department of Animal Science, North Carolina State University, NC Research Campus, PHHI building, 600 Laureate Way, Kannapolis 28081 – NC USA*
[e]*Department of Life Sciences and Biotechnology, University of Ferrara, Via Borsari 46, 441212, Ferrara, Italy*

Keywords

Antioxidant agents, Glycogen synthase kinase 3 beta (GSK-3β), Adenosine Kinase (AK), dual inhibitors, molecular docking

Corresponding authors:

*Federico Focher, Tel. +390382546352, email: focher@igm.cnr.it

*Stefania Butini, Tel. +390577234161, email: butini3@unisi.it

*Sandra Gemma, Tel. +390577234326, email: gemma@unisi.it

[1]These authors contributed equally to this work

Abstract

The manuscript deals with the design, synthesis and biological evaluation of novel benzoxazinone-based and indole-based compounds as multifunctional neuroprotective agents. These compounds inhibit *human* adenosine kinase (*h*AK) and *human* glycogen synthase kinase 3 beta (*h*GSK-3β) enzymes. Computational analysis based on a molecular docking approach underlined the potential structural requirements for simultaneously targeting both proteins' allosteric sites. *In silico* hints drove the synthesis of appropriately decorated benzoxazinones and indoles (**5a-s**, and **6a-c**) and biochemical analysis revealed their behavior as allosteric inhibitors of *h*GSK-3β. For both our hit **4** and the best compounds of the series (**5c**,**l** and **6b**) the potential antioxidant profile was assessed in human neuroblastoma cell lines (IMR 32, undifferentiated and neuronal differentiated), by evaluating the protective effect of selected compounds against H_2O_2 cytotoxicity and reactive oxygen species (ROS) production. Results showed a strong efficacy of the tested compounds, even at the lower doses, in counteracting the induced oxidative stress (50 μM of H_2O_2) and in preventing ROS formation. In addition, the tested compounds did not show any cytotoxic effect determined by the LDH release, at the concentration range analyzed (from 0.1 to 50 μM). This study allowed the identification of compound **5l**, as the first dual *h*AK/*h*GSK-3β inhibitor reported to date. Compound **5l**, which behaves as an effective antioxidant, holds promise for the development of new series of potential therapeutic agents for the treatment of neurodegenerative diseases characterized by an innovative pharmacological profile.

1. Introduction

Oxidative stress (OS) stems from an imbalance between the increase of the levels of reactive oxygen species (ROS), with respect to basal conditions, and the detoxification efficiency of the biological system in repairing eventual resulting damage [1]. OS is implicated in many pathologies and in several neurodegenerative diseases including Alzheimer's disease (AD), Parkinson's disease (PD), multiple sclerosis (MS) [2, 3], and amyotrophic lateral sclerosis (ALS) [4]. Although the etiology of these diseases is not fully elucidated, a series of seminal evidences have indicated OS as one of the potential hallmark common to different neurodegenerative diseases [5]. Chronic OS causes neuronal cell death by different mechanisms: moderate OS induces an apoptotic mechanism while acute OS causes necrosis [6]. For these reasons the identification of compounds able to prevent or lower cellular ROS formation is an intriguing task potentially endowing compounds with neuroprotective properties [7, 8]. Accordingly, the development of agents able to prevent neuronal cell death by inhibiting one or more enzymes involved in the neurodegenerative processes is a challenging task [9]. This is especially true for those diseases that are currently only symptomatically treated and for which a disease-modifying approach is highly desirable [10, 11].

Further, for the treatment of complex central nervous system (CNS) disorders and neurodegeneration where disease progression involves a wide number of biological systems, the development of multi-target directed ligands (MTDLs) is particularly advantageous [12-14] with respect to selective compounds (acting in a one-drug one-target fashion) [15]. In this view, efficient targeting of different pathways of a given disease by using only one molecule may improve therapeutic effectiveness [12, 14-16]. To support this hypothesis, besides a fine-tuning modulation of multiple G protein–coupled receptors (GPCRs) for attaining neuroprotection [17], dual enzyme inhibitors such as β-site amyloid precursor protein cleaving enzyme (BACE-1)/Glycogen Synthase Kinase 3β (GSK-3β) [18], cyclooxygenase-2 (COX-2)/5-lipoxygenase (5-LOX) [19], μ-calpain/cathepsin B [20], fatty acid amide hydrolase

(FAAH)/monoacylglycerol lipase (MAGL) have also been explored and/or proposed for the treatment of different brain disorders [21].

Human adenosine kinase (*h*AK, EC.2.7.1.20) and *human* glycogen synthase-3β (*h*GSK-3β, EC 2.7.11.26) are both involved in neurodegenerative disorders (such as AD and PD), and in the modulation of OS. Following our strong interest in the development of MTDLs [22] for different neurological [14, 23-25] and neurodegenerative diseases [11, 13, 26-30] we decided to explore the generation of dual inhibitors of *h*AK and *h*GSK-3β.

*h*GSK-3β is a constitutively active serine-threonine protein kinase, which plays a key role in several physiological processes ranging from glycogen metabolism to gene transcription. Its abnormal activity has been associated with some brain and neurodegenerative disorders such as schizophrenia, bipolar disorder, AD and PD [31]. Concerning AD, *h*GSK-3β over-activity accounts for memory impairment, tau hyperphosphorylation, increased amyloid beta (Aβ) production and local plaque-associated microglial-mediated inflammatory responses [32]. It was demonstrated that OS was able, in cultures of rat cortical neurons, to significantly increase tau phosphorylation by elevating the activity of GSK-3β [33]. It has been proposed that, either interaction of the Aβ with GSK-3β, or the Aβ mediated OS and ROS overproduction are able to activate GSK-3β. On the other hand, different studies have concluded that an increased functioning of GSK-3β may promote the β-secretase mediated Aβ formation. In any case, inhibition of GSK-3β may result beneficial for the treatment of AD [33]. More recently, *h*GSK-3β was also discovered to play a role in several cellular processes associated with the pathogenesis of PD, including the accumulation of α-synuclein aggregates, OS and mitochondrial dysfunction [34]. Furthermore, in neuronal hippocampal cell lines it was demonstrated that inhibition of GSK-3*β* is involved in the control of OS [35]. The seminal studies that clearly evidenced the link between GSK-3*β* and the modulation of OS have prompted the development of a series of GSK-3*β* inhibitors for the treatment of neurodegenerative diseases. Nevertheless it must be considered that over-inhibition of GSK-

3β might be deleterious since, by activating Wnt signaling, it would induce tumorigenesis through tumor necrosis factor toxicity. Accordingly, since it was demonstrated that optimal inhibition levels should be applied [36] we investigated an indirect modulation of GSK-3β by developing allosteric modulators.

*h*AK, which phosphorylates the nucleoside adenosine (Ado) to Ado monophosphate (AMP), plays an important role in modulating both intracellular and extracellular concentrations of Ado, which exerts autocrine and paracrine activity on cell physiology, via interaction with Ado receptors in the vicinity of its release site [37, 38]. It is relevant to the purpose of developing neuroprotective agents that Ado exerts a cytoprotective effect by enhancing the activities of antioxidant enzymes (e.g., superoxide dismutase, catalase and glutathione peroxidase) thus reducing the level of ROS [39]. On these bases inhibition of Ado catabolic enzymes such as AK may allow to elicit these beneficial effect on OS. Recent studies report that abnormal Ado concentrations are involved in some diseases affecting central and peripheral nervous systems (CNS, PNS) such as schizophrenia, epilepsy, AD, Huntington's disease, ALS, and MS, where the fine-tuning of Ado concentration by *h*AK inhibition appears physiologically relevant [40, 41]. The role of the inhibition of both enzymes for the treatment of neurodegenerative disorders, and their converging efficacy in the control of OS suggested *h*AK and *h*GSK-3β as suitable targets for the development of innovative MTDLs endowed with neuroprotective properties. A further support to the rational for developing dual inhibitors stemmed from the analysis of the structure of both enzymes.

We recently described the development of allosteric inhibitors for *h*AK [42, 43] while selective allosteric modulators of *h*GSK-3β [44], by targeting sites distinct from the ATP binding site, have been described by others [45-47].

Aiming at developing the first *h*AK/*h*GSK-3β dual inhibitors with potential neuroprotective properties, our analysis started from the investigation of the chemical structure of known allosteric inhibitors of *h*AK or *h*GSK-3β exemplified by NSD438 (**1**) [42], VP0.7 (**2**), [45] and benzothiazinone **3** [47] (Figure 1) for retrieving the common structural determinants for allosteric inhibition of both enzymes. A preliminary

biological test to assess *h*GSK-3β inhibition potency on a selected panel of our in house database allowed us to select compound **4** [48] (Figure 1) as a 16 μM *h*GSK-3β inhibitor. Starting from **4** and taking into account our knowledge on the allosteric modulation of *h*AK, by combining synthetic, molecular modeling and biological efforts we identified the benzoxazinone as a promising scaffold for *h*AK/*h*GSK-3β dual inhibition (compounds **5a-s**, Figure 1 and Table 1). In more details, a medicinal chemistry approach was based on bioisosteric ring contraction of the seven membered ring of the pyrrolobenzoxazepine system of **1** and the transformation of the keto functionality in the lactam of the benzoxazinones **5a-s** with a bicyclic scaffold that mimics that of compound **1**. An aromatic system attached to the lactam nitrogen, mainly represented by an *N*-benzyl-substituted system as in **3**, could serve as mimetic of the pyrrole-fused system of **1**. A further ring contraction of compounds **5a-s** was achieved with the indole-based inhibitors (**6a-c**). These newly conceived scaffolds also allowed improving synthetic feasibility and chemical tractability by removal of chiral centers. All the developed compounds were investigated as dual inhibitors of *h*AK and *h*GSK-3β.

To characterize the potential neuroprotective profile of the developed compounds (**4, 5c,l** and **6b**), the cellular effects on cytoprotection and OS modulation were evaluated on the human neuroblastoma cell line IMR 32. As observed none of the compounds showed a cytotoxic effect as determined by LDH release. In addition, compounds **4**, **5c**,**l** and **6b** were effective in preventing ROS production after H_2O_2 treatment in IMR 32 cells. Among this new class of compounds derivative **5l** stood out and represents the first *h*AK/*h*GSK-3β dual inhibitor reported to date which is also able to counteract OS in neuroblastoma cell lines. This compound will pave the way to the discovery of a new class of multifunctional drugs as potential neuroprotective agents.

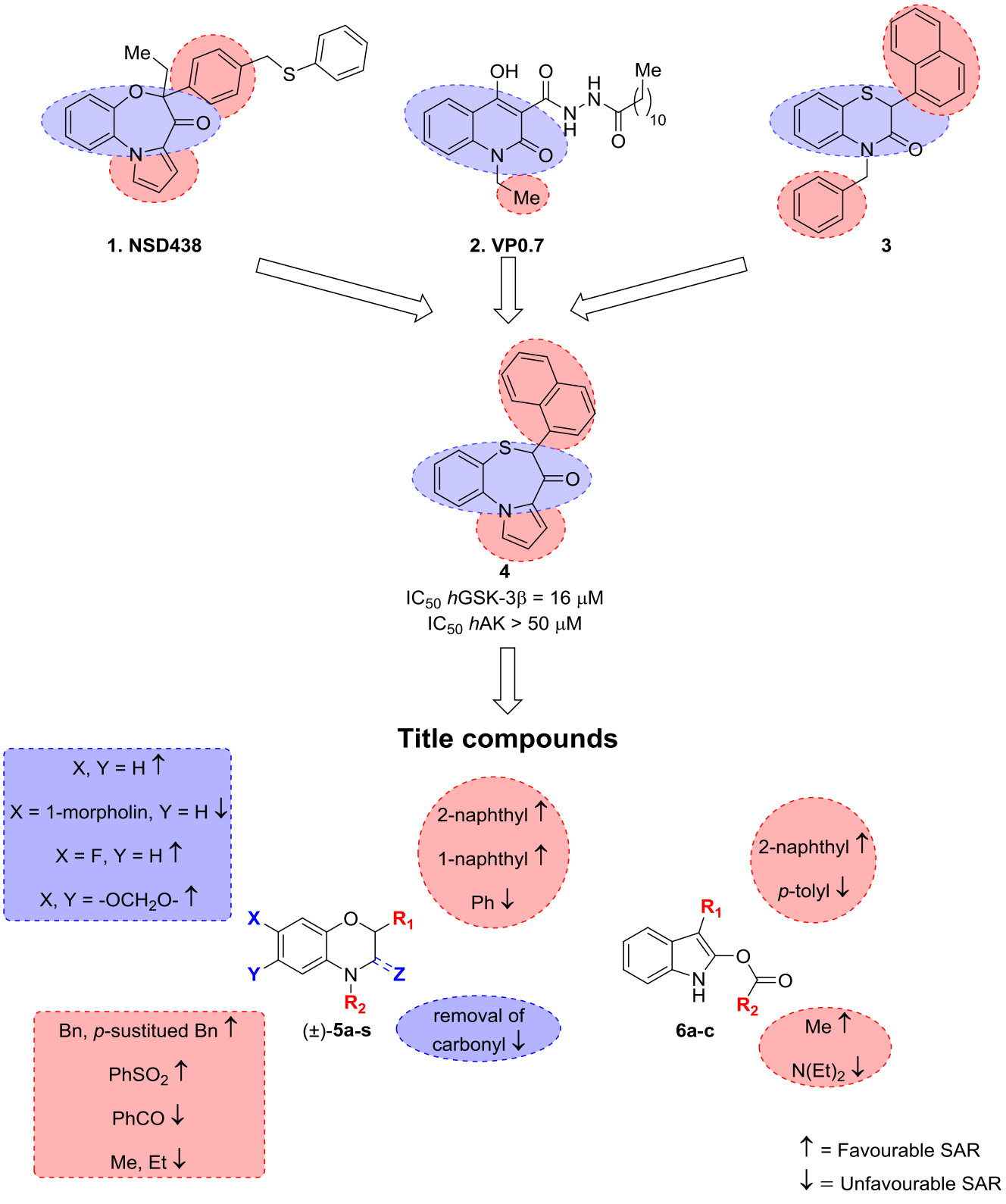

Figure 1. Outline of the rational design of *h*AK/*h*GSK-3β dual allosteric inhibitors **5a-s** and **6a-c** (structures are defined in Table 1).

2. Results and Discussion

2.1. Chemistry

The compounds **5a-s** and **6a-c** were synthesized as described in Schemes 1-4. Briefly, condensation of 2-aminophenol **7** with α-bromonapthyl ester **8a** or **8b** in the presence of K_2CO_3 gave the benzoxazinone derivatives **9a,b** that were *N*-alkylated with the appropriate benzyl bromide (Scheme 1) to afford the compounds **5a-g** (Table 1). Reduction of **9a** with BH_3SMe_2 in THF gave the corresponding benzoxazine **10**, which was reacted with benzoyl chloride or benzenesulfonyl chloride to obtain **5h** and **5i** respectively (Scheme 1). The benzoxazinones **13a-e** (Table 1) were prepared from O-alkylation of appropriate 2-nitrophenol derivatives **5j-s** with α-bromonapthyl ester **8a** or **8b** or α-bromophenyl ester **8c** to provide the corresponding intermediates **12a-e** (Scheme 2). Subsequent reduction of **12a-e** afforded the corresponding aniline derivatives which spontaneously cyclized to benzoxazinone analogues **13a-e**. Finally, **13a-e** were *N*-alkylated with the appropriate benzyl/alkyl halides to furnish the title compounds **5j-s** (Table 1). The synthesis of 6-nitrobenzo[1,3]dioxol-5-ol **11c** was accomplished in three steps, as depicted in Scheme 3. In detail, commercially available sesamol **14** was converted in its acetyl analogue **15**, that was nitrated with HNO_3/AcOH [49] to give the acetic acid 6-nitrobenzo[1,3]dioxol-5-yl ester **16**. Then, after hydrolysis of **16** with 20% (v/v) H_2SO_4, the 6-nitrobenzo[1,3]dioxol-5-ol **11c** was obtained in good yield.

The synthesis of indole-based compounds (**6a-c**, Scheme 4) started with isatine **17** which, after treatment with sodium hydride, generated the sodium isatinate intermediate which was subjected to a Grignard reaction with the appropriate aryl bromide magnesium salt for obtaining the intermediate carbinols (**18a,b**). These latter were immediately dehydroxylated by means of a tin(II)chloride reduction and the obtained indolinones (**19a,b**) were treated with acetyl chloride or diethylcarbamoyl chloride providing the esters **6a,b** and the carabamoyl analogue **6c**.

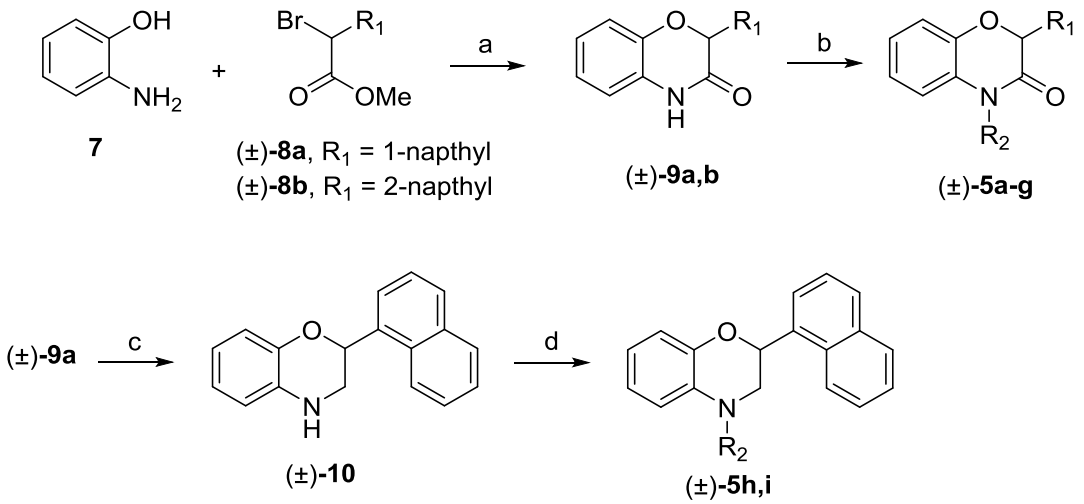

Scheme 1. *Reagents and conditions:* a) K_2CO_3, dry DMF, 100 °C; b) Cs_2CO_3, dry DMF, rt, R_2Br; c) BH_3•SMe_2, dry THF, rt, 12 h; d) benzoyl chloride (for **5h**) or benzenesulfonyl chloride (for **5i**) TEA, dry dichloromethane (DCM), rt, 12 h.

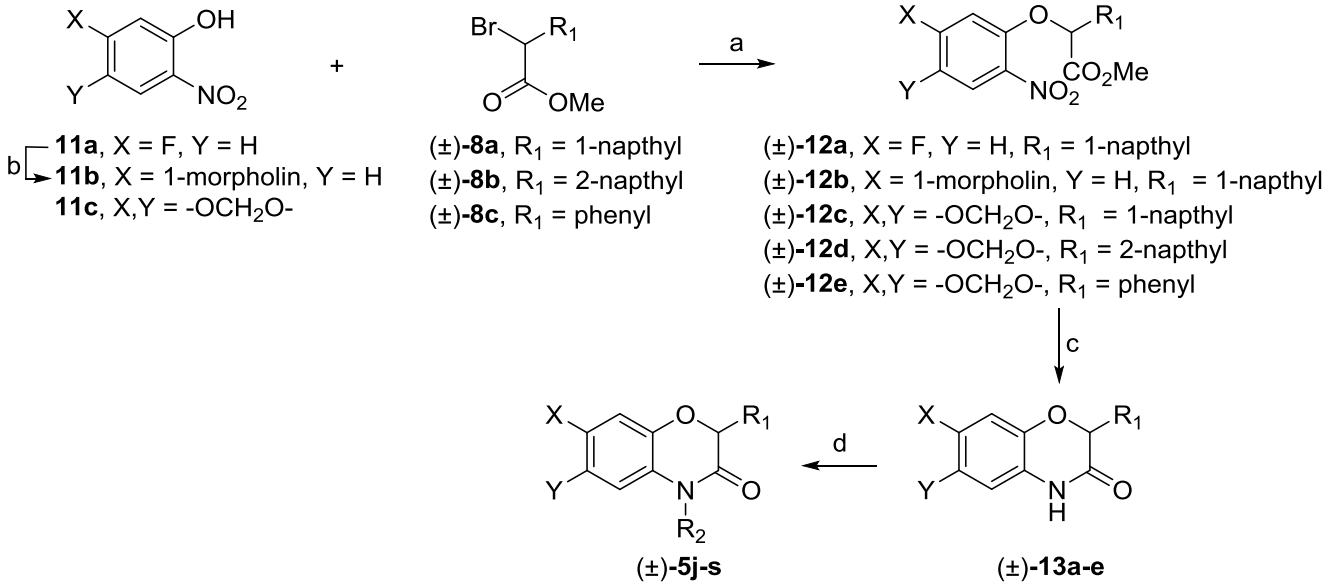

Scheme 2. *Reagents and conditions*: a) K_2CO_3, dry DMF, rt, 12 h; b) morpholine, MeCN, reflux [50]; c) Fe/NH_4Cl/THF/H_2O, 100 °C (for **13a,b**) and $SnCl_2$/EtOH, 80 °C (for **13c-e)**; d) Cs_2CO_3, DMF, appropriately *p*-substituted benzylbromide, rt.

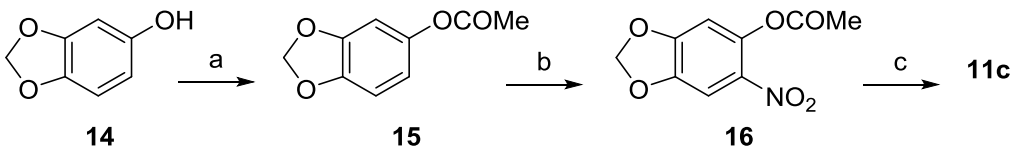

Scheme 3. *Reagents and conditions*: a) Ac_2O, NaOH, 0 °C to rt; b) HNO_3c/AcOH, rt; c) 20% H_2SO_4.

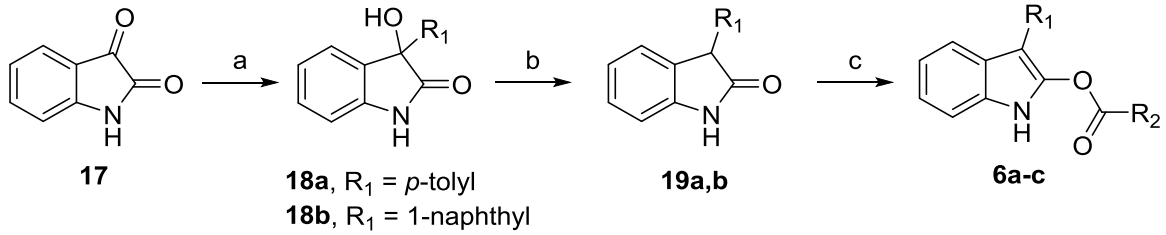

Scheme 4. *Reagents and conditions*: a) NaH (60% slurry in mineral oil), *p*-tolylmagnesium bromide (1 M in THF) (for **18a**) or 1-naphthylmagnesium bromide (for **18b**), dry THF, from -15 °C to rt, then rt 14 h; b) $SnCl_2$, AcOH, HCl, 115 °C, 2.5 h; c) 2,6-lutidine and AcCl (for **6a,b**) or diethylcarbamoyl chloride (for **6c**), dry DCM, from 0 °C to rt, then rt 16 h.

2.2. Enzymatic studies, molecular modelling, and structure-activity relationships (SAR)

2.2.1. Enzymatic inhibition

The inhibition effect of our compounds on *h*GSK-3β and *h*AK activity was examined over a range of inhibitors' concentrations in the assay conditions reported in Methods section, where labeled ATP (10 μM) or Ado (1 μM) are in their respective K_M concentrations. Table 1 shows the IC_{50} values of the compounds on both enzymes.

Since our aim was to rationally design molecules potentially able to inhibit both enzymes, we have tested on *h*AK the compounds that showed the best inhibition potential against *h*GSK-3β (Table 1).

Table 1. Inhibitory activity of compounds **4**, **(±)-5a-s**, and **6a-c** against *h*AK and *h*GSK-3β (IC_{50}, μM).

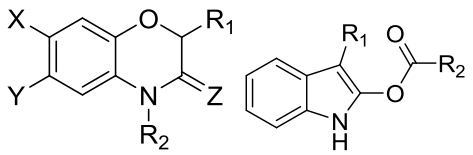

5a-s **6a-c**

Cpd	R_1	R_2	X	Y	Z	*h*AK IC_{50} (μM)[a] (%)[b]	*h*GSK-3β IC_{50} (μM)[a] (%)[b]
1						1.2[c]	NT[d]
4	-	-	-	-	-	> 50 (33)	16
(±)-5a	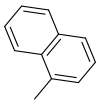		H	H	O	NT[d]	> 50 (48)
(±)-5b		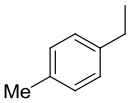				NT[d]	50
(±)-5c		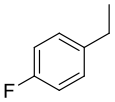				40	5.4
(±)-5d		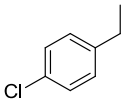				NT[d]	> 50 (46)
(±)-5e		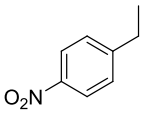				NT[d]	> 50 (40)
(±)-5f		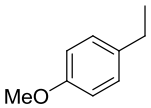				31.6	8.1 ± 1.8
(±)-5g	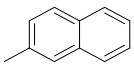	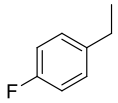	H	H	O	32.2	8.7 ± 1.8
(±)-5h	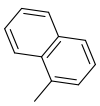	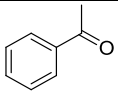	H	H	H,H	NT[d]	> 50 (25)
(±)-5i		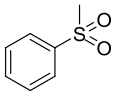				57.4	4.1 ± 0.3
(±)-5j	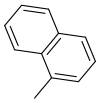	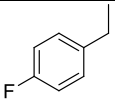	F	H	O	24.7	21.2 ± 6.3
(±)-5k	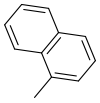	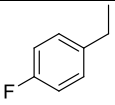		H	O	> 50	10.1 ± 2.8

(±)-5l						13.6	6.4
(±)-5m	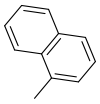	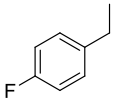	-OCH_2O-		O	> 50 (12)	8.1 ± 0.8
(±)-5n		Me				> 50 (12)	> 50
(±)-5o		Et				> 50 (8)	25.6
(±)-5p	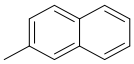		-OCH_2O-		O	13.7	6.9 ± 1.5
(±)-5q						> 50 (40)	50
(±)-5r		Me	-OCH_2O-		O	> 50 (10)	> 50 (8)
(±)-5s		Et				> 50 (5)	> 50 (15)
6a	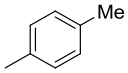	Me	-	-	-	50	50
6b	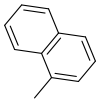	Me	-	-	-	13.6	10
6c	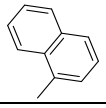	$N(Et)_2$	-	-	-	NT[d]	> 50 (38)

[a]Each value is the mean of at least three determinations, standard error of the mean is ≤ 15%; [b]inhibition % when tested at 50 μM; [c]from ref [40]; [d]NT, not tested.

Earlier studies demonstrated that our pyrrolobenzoxazepine-based compounds, typified by **1**, inhibit *h*AK in a non-competitive manner. We also hypothesized and demonstrated by mutagenesis studies that the specific interaction site of these compounds could be identified in *h*AK in an allosteric pocket close to the active site [42, 43] and placed in close proximity of the enzyme surface.

In order to identify a potential binding site on *h*AK for the class of compounds **5** and **6**, we carried out a blind docking calculation considering *h*AK in its closed form (PDB ID: 1BX4) and both enantiomers of **5l**. For this computational analysis AutoDock [51] software has been used. AutoDock software is able to perform the blind docking of compounds and to select the correct complexes based on energy without

previous data regarding the binding site. The results of AutoDock *in silico* experiment are reported in Figure 2. In particular the output regarding the (*R*)-**5l** is reported in Figure 2A, while the output of (*S*)-**5l** enantiomer is reported in Figure 2B. The data analysis clearly evidences that the favorite binding site, on *h*AK enzyme, for the lower energy poses of both enantiomers of **5l** is the allosteric site previously identified for the compound **1** [42, 43], while only few docked solutions in the considered range (see the Experimental section for details) were found to be in different sites with respect to the above-mentioned allosteric site. Moreover only docked poses possessing much less favorable docking scores and predicted ligand affinities, when compared to those found for **5l** into *h*AK allosteric binding site, were found in the ATP binding site. Additionally, for both enantiomers, no poses were found in the Ado binding site. According to our computational investigation, both the binding sites for Ado and ATP, as well as other potential sites located at the surface of the enzyme, appeared not suitable for **5l**-*h*AK interactions. In fact, we retrieved not favorable docking scores and predicted ligand affinities for these sites which only accommodated conformers with predicted activity > 30 μM. Overall, we hypothesized the *h*AK allosteric site as the most reliable binding site for **5l** and its analogues.

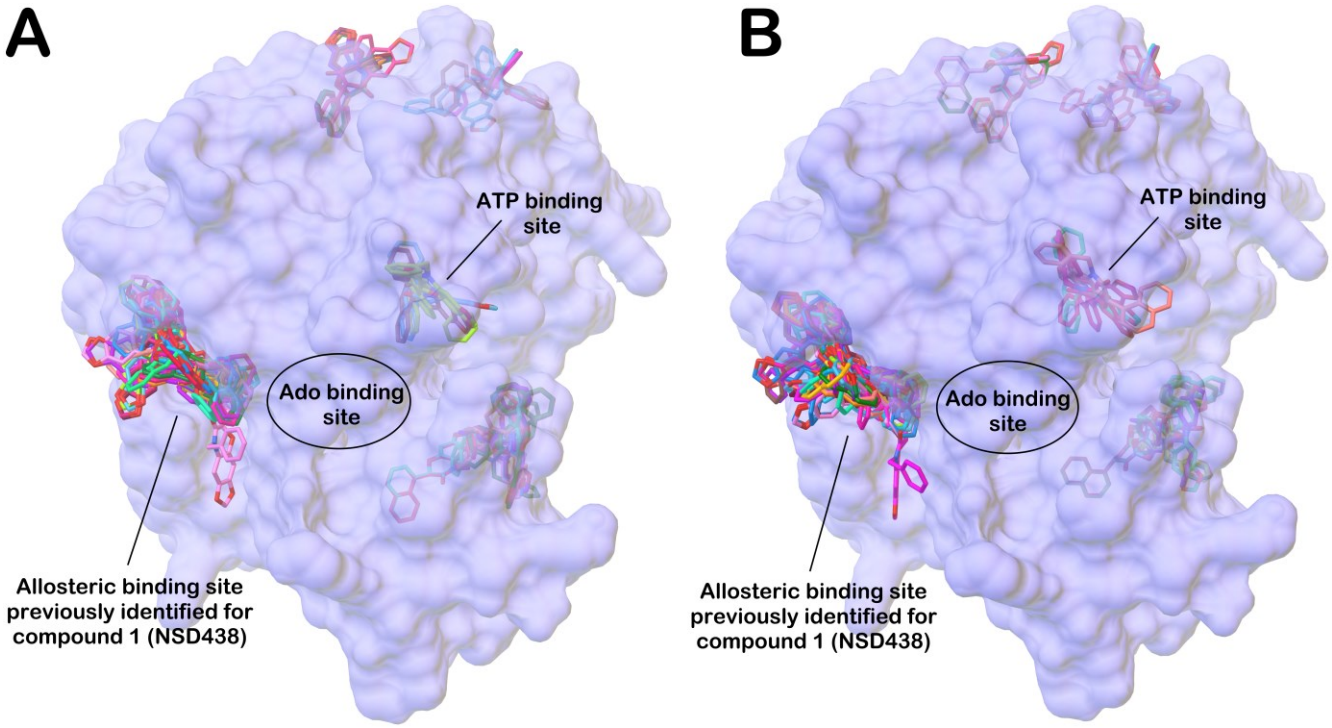

Figure 2. Blind docking output for (*R*)-**5l** (A) and (*S*)-**5l** (B) of (colored sticks) against *h*AK (light blue surface). In the picture are highlighted the main identified binding sites. The picture was generated by AutoDockTools.

Thus, in order to test their mechanism of action also on *h*GSK-3β, we assayed two compounds representative of the series, namely **5c** and **5l**, at different concentrations of the phosphate donor ATP. We found out that the compounds inhibit the enzyme by a non-competitive mechanism, interacting with either the enzyme or the enzyme-substrate complex, decreasing the rate of the enzyme catalytic activity, without modification of the dissociation constant for the substrate/enzyme complex. As shown in Figure 3, by increasing the concentrations of the inhibitors the value of V_{max} decreases to a new value called $V_{app\ max}$. In contrast with V_{max}, K_M for ATP is not affected, remaining close to 10 μM at each inhibitor concentration, indicating for both **5c** (Figure 3, Panel A) and **5l** (Figure 3, Panel B) a non-competitive inhibition.

Finally, through the formula $K_i = [I]/(V_{max}/V_{app\ max} - 1)$, we confirm for **5c** and **5l** K_i value equal to IC_{50} values, namely 5.6 ± 1.0 and 6.3 ± 1.5 μM, respectively

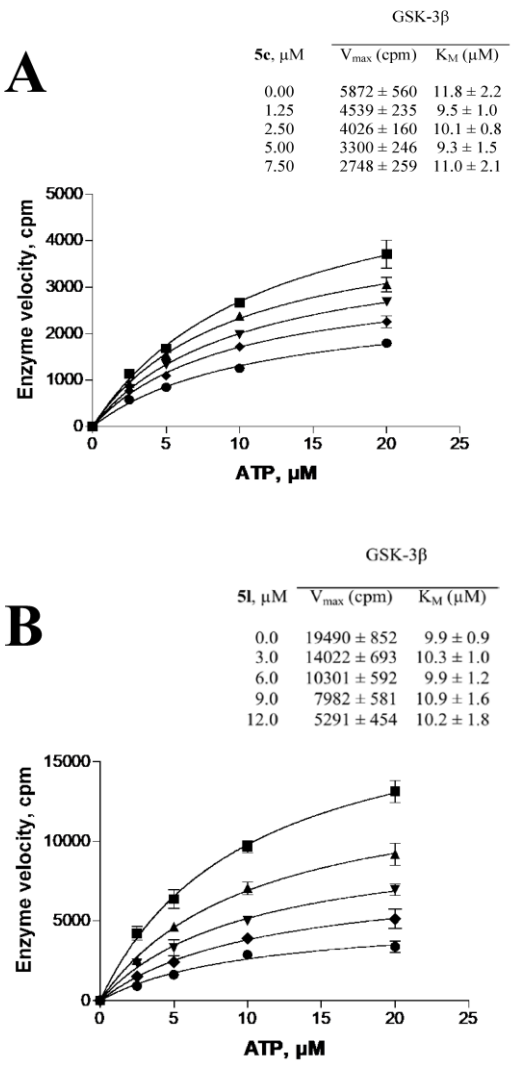

Figure 3. Effect of increasing concentrations of **5c** (Panel A) and **5l** (Panel B) on *h*GSK-3β activity, at different [^{33}P]-ATP concentrations. **5c** concentrations: (■) 0.0, (▲), 1.25, (▼) 2.5, (◆) 5.0, (●) 7.5 μM. **5l** concentrations: (■) 0.0, (▲), 3.0, (▼) 6.0, (◆) 9.0, (●) 12.0 μM. V_{max} and K_M at each inhibitor concentration were determined with Prism3 software through the formula Y = X* V_{max} /(K_M +X).

Based on the biological results and on enzyme computational analysis, taking into account the pharmacophore similarity of **5a-s** and **6a-c** with **2** and **3**, we hypothesized that the new compounds may bind the allosteric site targeted by compound **2** [45] on *h*GSK-3β (see Figures S1-S3 of the Supplementary Material).

Accordingly the designed compounds were subjected to molecular docking studies into the two postulated allosteric sites to verify the relevant interactions responsible for the dual-target profile and support structure–activity relationships studies (SARs) and optimization process. In general the results of the docking studies were consistent with the biochemical studies (determination of the inhibition potencies of the racemic compounds against *h*AK and *h*GSK-3β reported in Table 1).

A systematic and comprehensive SAR study of the developed compounds **5a-s** and **6a-c** started from compound **4** (Ki *h*GSK-3β = 16 μM; Ki *h*AK > 50 μM). We investigated the potential substitutions able to improve the binding of compound **4** within the allosteric cavities of the target enzymes following our docking output indications (Figure S1A and B for (*R*)-**4** and (*S*)-**4**, respectively). Based on known *h*GSK-3β inhibitors' structure the pyrrole moiety was removed and replaced by hydrophobic bulky and flexible groups while the benzoxazinone system was decorated by different substituents. The putative binding modes of the dual inhibitors were investigated using a computational protocol based on the Induced Fit Docking (IFD) technique [24, 28, 52]. As better detailed in the experimental section we used human enzymes for the docking protocols (*h*AK, PDB ID: 1BX4; *h*GSK-3β, PDB ID: 1HF8).

The IFD output obtained with the (*S*)- and (*R*)-enantiomers within *h*AK and *h*GSK-3β binding sites for the best performing dual *h*AK/*h*GSK-3β inhibitors **5c** and **5l** is depicted in Figures 4 and 5 respectively. Although the enantiomers of each compound were found to mainly target conserved residues, we noted the lack of a stereoselective mode of interaction with the putative allosteric binding sites with slight differences in terms of number of contacts. This was in agreement with previous results on *h*AK [42, 43].

(*R*)-**5c** and (*S*)-**5c** bind *h*AK (Figure 4 panels A and B, respectively) by H-bonding the backbone of F338 with the carbonyl group of the benzoxazinone scaffold. This latter also stacked with W75 and H107 residues. The naphtyl moiety was able to establish hydrophobic interactions and a cation-π stacking with the sidechain of K71.

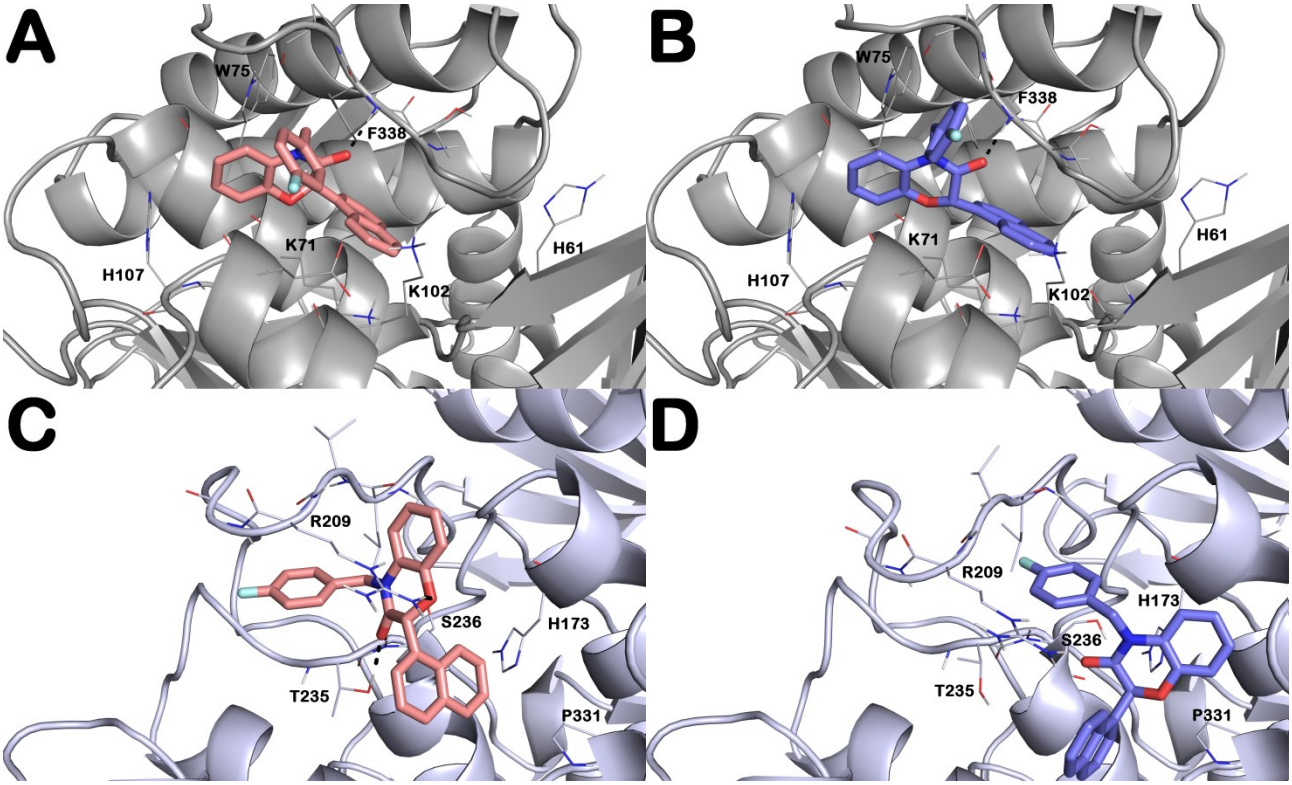

Figure 4. IFD output of compound **5c**: (*R*)-**5c** and (*S*)-**5c** into *h*AK (panels **A** and **B**; respectively) and *h*GSK-3β (panels **C** and **D**; respectively). H-bonds are reported as black dotted lines. Pictures were generated by PyMOL. Nonpolar hydrogen atoms were omitted for the sake of clarity.

When **5c** was docked into the allosteric site of *h*GSK-3β, although the binding modes of the two enantiomers were slightly different, we noted similar pattern of residues involved in the interactions with the compound. Furthermore, (*R*)-**5c** (Figure 4C) was accommodated within a cleft where the contacts with R209 mainly govern the retrieved binding modes. Compound **5c** established hydrophobic

interactions such as cation-π stacking, and also an H-bond between the bridged oxygen of the benzoxazinone nucleus and the sidechain of R209. The benzoxazinone carbonyl group formed polar contacts with the sidechain of T235. The naphthyl moiety formed a strong network of hydrophobic interactions with H173 (π -π stacking) and P331. On the contrary, the docked pose of (*S*)-**5c** (Figure 4D) was mainly characterized by hydrophobic contacts. Indeed, the benzoxazinone moiety of (*S*)-**5c** was differently accommodated to strongly interact by a double π -π stacking with H173. This event hindered the formation of the above-noted H-bonds with T235 and R209, in favor of more productive hydrophobic interactions with the P331 sidechain. For this enantiomer the *p*-F-benzyl moiety was deeply positioned into the allosteric site of *h*GSK-3β interacting with the loop containing residue R209, by hydrophobic interactions (Figure 4D).

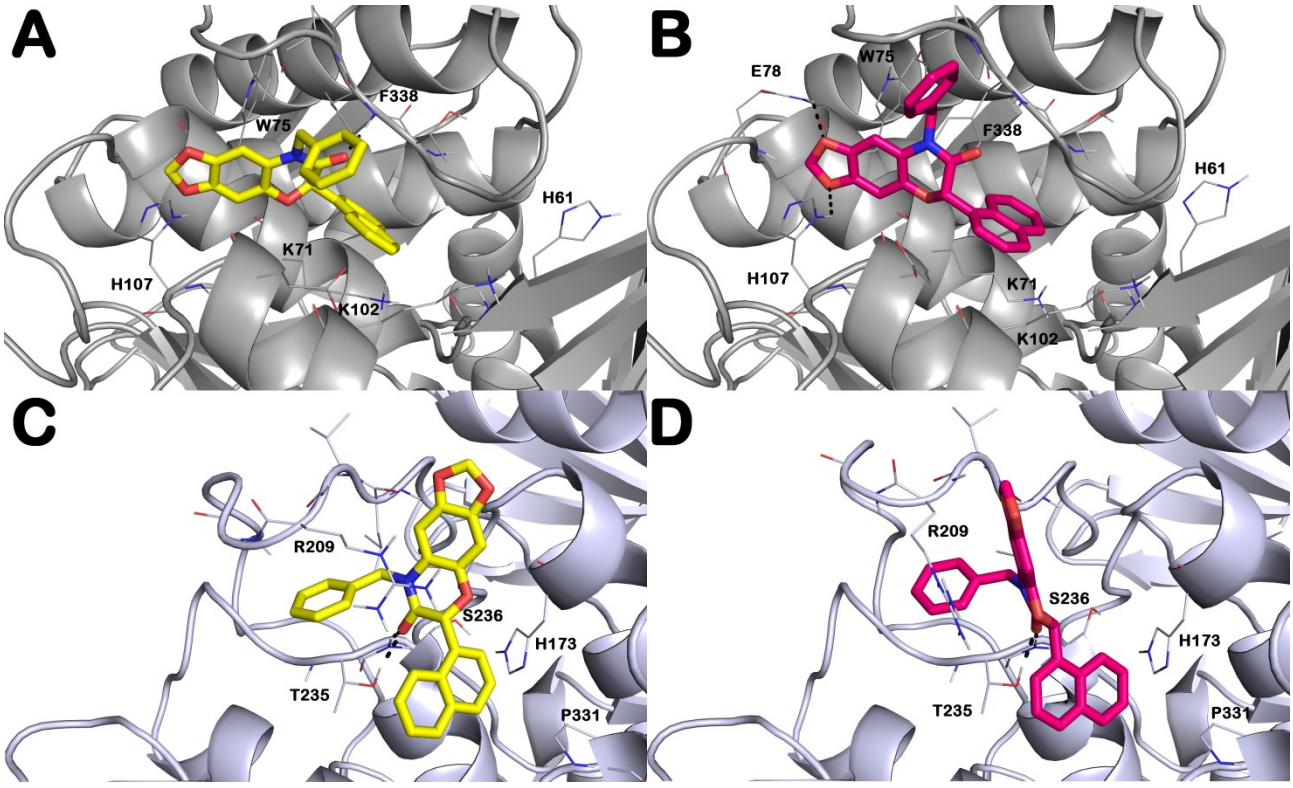

Figure 5. IFD output of compound **5l**: (*R*)-**5l** and (*S*)-**5l** into *h*AK (panel **A** and **B**; respectively) and *h*GSK-3β (panel **C** and **D**; respectively). H-bonds are reported as black dotted lines. Pictures were generated by PyMOL. Non polar hydrogen atoms were omitted for the sake of clarity.

Docking studies with compound **5l** into the *h*AK allosteric site showed that it could establish a series of polar and hydrophobic contacts. In particular, (*R*)-**5l** (Figure 5A) formed an H-bond with the residue F338 (backbone) by the oxygen of the carbonyl group. The tricyclic system can establish a series of relevant interactions such as a π-π stacking with W75 by its aromatic moiety, a relevant hydrophobic interaction with H107 by its dioxole ring and an H-bond with the backbone of F338 by the oxygen of the carbonyl group.

Moreover, the naphthyl group was able to establish hydrophobic interactions and a cation-π stacking with the sidechain of K71. The enantiomer (*S*)-**5l** (Figure 5B) was differently accommodated allowing H-bonds with residues E78 and H107. Furthermore, it was able to strongly interact with the binding site by an improved network of hydrophobic interactions with respect to (*R*)-**5l**. Besides the previously described π-π stacking with W75 and hydrophobic interactions with H107, the naphthyl moiety established a cation-π stacking with K71 and a π-π stacking with F338.

Regarding the docking outputs of **5l** into *h*GSK-3β (Figure 5), we observed that the compound was able to bind the allosteric cavity in a similar fashion to that already reported for compound **2**, targeting a series of key residues by hydrophobic and polar contacts [45]. Furthermore, after analyzing the docking output of (*R*)- and (*S*)-**5l** enantiomers (Figure 5 panels C and D, respectively) we found very limited differences. In particular, the main contacts of the compound were established with R209 (cation-π stacking) by the tricyclic moiety. Other polar contacts could be formed by our ligand and the sidechain or backbone of T235 and S236, respectively for both enantiomers. In addition, the naphthyl moiety established hydrophobic interactions with H173 (π-π stacking), and P331.

Starting from **5a** (Figure S1C and D for (*R*)-**5a** and (*S*)-**5a**, respectively), bearing a "naked" benzyl group, the *p*-position of the benzyl system was explored with compounds **5b-f** by introducing electron-withdrawing (EWGs) or electron-donating groups (EDGs) such as Me, F, Cl, NO_2 and OMe, also characterized by different shapes and steric hindrance. Introduction of a Me group (**5b**), led to a lack of activity against *h*GSK-3β (Figure S1E and F for (*R*)-**5b** and (*S*)-**5b**, respectively). Also the introduction of a *p*-Cl (**5d**) (Figure S1G and H for (*R*)-**5d** and (*S*)-**5d**, respectively) or a *p*-nitro group (**5e**) (Figure S1I and J for (*R*)-**5e** and (*S*)-**5e**, respectively) caused a dramatic fall of the activity. These data support the hypothesis that small substituents at *p*-position such as H and F may be better tolerated by the *h*GSK-3β allosteric binding site, and may promote a binding mode as that retrieved for **5c**. Introduction of a *p*-methoxy as in **5f** led to a compound with a similar pattern of interactions as for **5c** with the allosteric binding site. In addition **5f** is able to form, with the oxygen of *p*-methoxy group, an H-bond with the backbone of G210. This binding mode accounted for a similar docking score as well as the activity against *h*GSK-3β (Figure S1K and L for (*R*)-**5f** and (*S*)-**5f**, respectively).

Further, for exploring a different region of the benzoxazinone scaffold, 2-naphthyl regioisomer was evaluated (**5g** vs **5c**) and this modification was well tolerated by both enzymes (Figure S1M and N for (*R*)-**5g** and (*S*)-**5g**, respectively).

Shifting the lactam carbonyl group to the exocyclic position (**5h**) resulted in a complete loss of potency indicating the need of a specific geometry of the bicyclic system for correct interaction (Figure S1O and P for (*R*)-**5h** and (*S*)-**5h**, respectively). On the other hand, when the amide carbonyl group of **5h** is replaced by a phenylsulfone group (**5i**), this latter is able to mimic the interaction with T235 and/or S236, already described for **5c** (Figure 4), **5f**, and **5g**. As expected, the binding mode of **5i** accounted for a similar inhibitory potency against *h*GSK-3β as found for **5c**. Moreover, also for **5i** the rings of the central core established a cation-π stacking with R209 (Figure S1Q and R for (*R*)-**5i** and (*S*)-**5i**, respectively).

Consistent with the positive contribution given by the small F substituent seen in **5c**, we inserted a F atom at C7 of the benzoxazinone moiety. This modification was well tolerated and for **5j** we registered a good inhibition profile for both enzymes paralleled by a favorable docking score (Figure S2A and B for (*R*)-**5j** and (*S*)-**5j**, respectively). The introduction of a morpholine (**5k**) at C7 of the heterocyclic system caused a slight decrease of activity against both *h*GSK-3β and *h*AK, due to the poorly tolerated steric hindrance at this position (Figure S2C and D for (*R*)-**5k** and (*S*)-**5k**, respectively).

Since the introduction of small substituents at C7 was tolerated, our next docking outputs prompted us to modify C7 and C8 of the benzoxazinone system. By adding a dioxole moiety to the scaffold of **5a**, we obtained one of our best performing compounds (**5l**) in terms of computational and biological results.

Based on these results we decided to investigate this tricyclic scaffold by introducing the same substitutions as in **5a**. As already observed, the introduction of a 2-naphthyl moiety (**5p**) implied minor changes in the inhibitory activity, and preserved a favorable binding mode into the *h*GSK-3β allosteric site (Figure S2E and F for (*R*)-**5p** and (*S*)-**5p**, respectively). On the contrary, the addition of the *p*-F on the benzyl group (**5m**) did not led to the positive increment as registered for the first series of compounds (Figure S2G and H for (*R*)-**5m** and (*S*)-**5m**, respectively).

In order to explore the hydrophobic substitution at 4 position of the tricyclic system we replaced the benzyl moiety with the smaller Me (**5n**) (Figure S2I and J for (*R*)-**5n** and (*S*)-**5n**, respectively) and Et (**5o**) (Figure S2K and L for (*R*)-**5o** and (*S*)-**5o**, respectively) substituents. The absence of the aromatic group in the central core determined the loss of a favorable 3D-arrangement in both enzymes with a consequent loss of activity of both compounds (**5n** and **5o**).

Since the 2-naphthyl substitution was well tolerated at 2 position, we explored the effect of the simplification of the aromatic system by removing one of the aromatic rings. The phenyl substituted analogue (**5q**) showed a different accommodation into the *h*GSK-3β allosteric binding site (Figure S2M and N for (*R*)-**5q** and (*S*)-**5q**, respectively). When compared to the pose obtained for **5l** we observed that,

due to the smaller size of the hydrophobic moiety, the key H-bonds were lost establishing hydrophobic contacts with the side chain of the R209. The presence of the phenyl moiety at C2 was then explored in combination with the replacement of the benzyl group, with Me (**5r**) (Figure S2O and P for (*R*)-**5r** and (*S*)-**5r**, respectively) and Et (**5s**) (Figure S2Q and R for (*R*)-**5s** and (*S*)-**5s**, respectively), as done for **5n** and **5o**. This led to compounds characterized by different binding modes and by a relevant decrease of inhibitory activity against *h*GSK-3β.

With the aim of simplifying the central scaffold we developed indole-based analogues devoid of a chiral centre but still able to establish the same contacts identified for the benzoxazinone-based compounds. Consistent with our hypothesis analogue (**6b**) bearing a 1-naphthyl substituent showed a satisfactory binding mode into the *h*GSK-3β allosteric binding site (Figure S3A-C for **6a-c**, respectively), confirmed by biological assays. This compound is able to stack with the R209 and to make polar contacts with the backbone of Y234, V208 and G210, sharing the pharmacophoric elements, previously described for **5c**, for interacting in both enzymes. This binding mode accounted for the best IC_{50} against both *h*AK and *h*GSK of the indole-based series.

2.3. Cytotoxicity evaluation and studies for evaluating antioxidant potential

Since OS is one of the main causes of neurodegeneration and is a relevant issue in a variety of neurological diseases we investigated the therapeutic potential of our dual inhibitors of *h*AK/*h*GSK-3β. To this end we decided to test the efficacy of compounds **4**, **5c**,**l** and **6b** in an acute model of OS induced by H_2O_2 treatment in both, differentiated and not differentiated IMR 32 cells.

Our test started by engaging the selected compounds in preliminary studies for determining their cytotoxicity profile by using IMR 32 cells. Accordingly, IMR 32 cells were treated with increasing concentrations of the tested compounds and cell vitality was then assessed by LDH release (see

Supplementary Material for further details). Preliminary studies allowed us to define the correct cell density to be used which was chosen on the base of cellular confluence 24 h after the seeding. The optimal number of cell seeded was 100,000 cells/well, as shown Figure S4 of the Supplementary Material. The cytotoxicity assessment (Figure 6) clearly showed that no cytotoxic effect among the 6 different doses tested was observed. Of note is that compound **4**, at the doses of 10 and 50 μM, clearly affect the cellular clusters formation (Figure S5) although **4** was found devoid of toxicity to the cells. No significant effects on IMR 32 cellular morphology were observed after compounds treatment, as reported Figure S5.

In summary, none of the tested molecules showed any cytotoxic effect on the adopted cellular model in the wide range of doses chosen (from 0.1 μM to 50 μM). These results allowed us to perform further experiments to evaluate their potential antioxidant properties against H_2O_2 treatment.

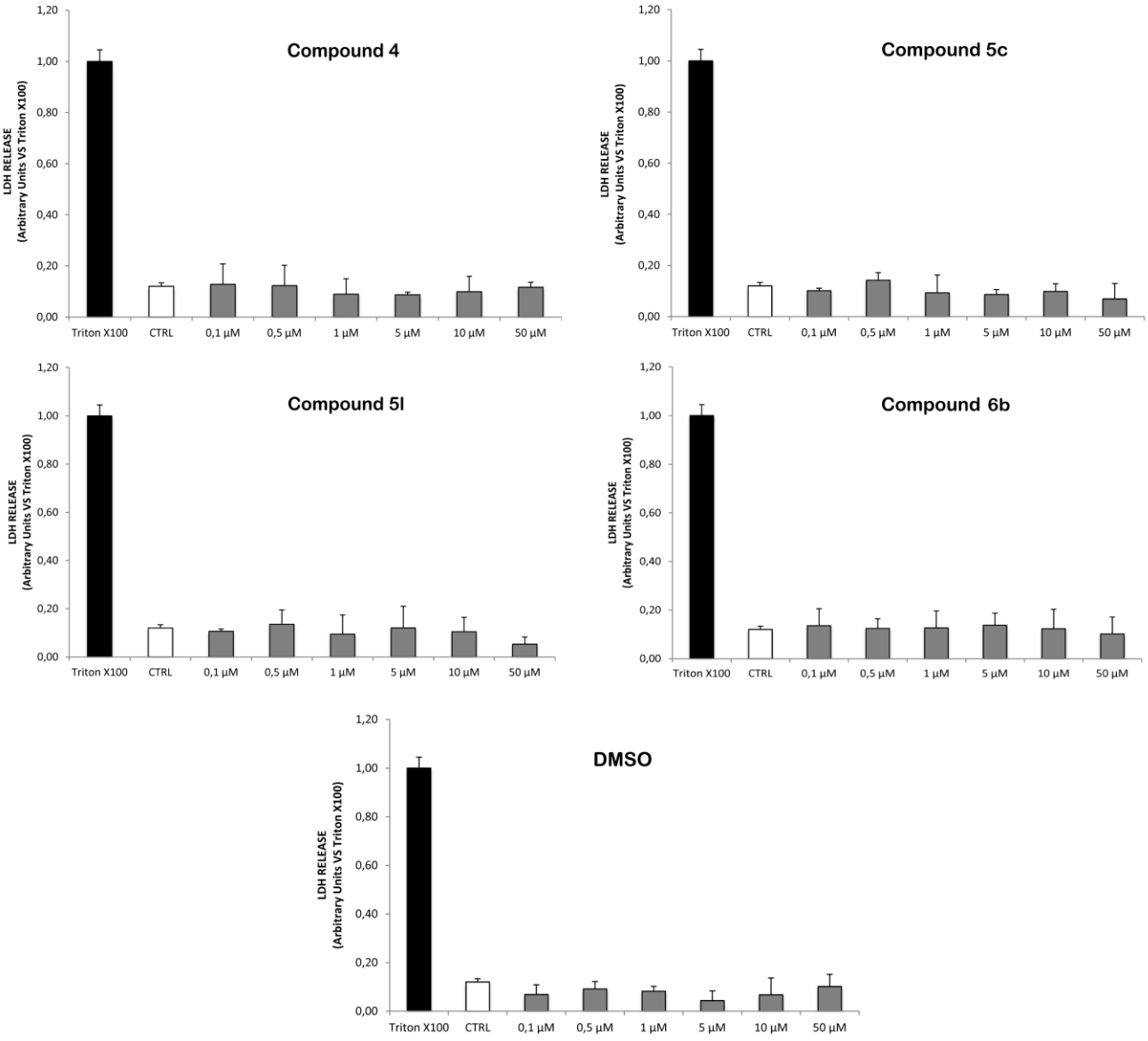

Figure 6. Cytotoxic effect of compounds **4**, **5c**,**l** and **6b**. Values represent average ± SD for three experiments in triplicate. Data are expressed as arbitrary unit LDH release as compared to the maximum release of LDH from Triton X-100- treated cells.

Following our plans we then evaluated the cytotoxicity of different doses of H_2O_2 (25, 50 and 100 µM) (Figure S6A). Further experiments were performed with 50 µM of H_2O_2, since it was the highest dose that did not affect dramatically cells morphology and viability, indeed with 100 µM treatment the LDH release paralleled the one of Triton X-100 (100% of cells damage) (Figures S6A and S6B).

Further, the levels of ROS by DCF probe were determined. As shown in Figure S7, we could observe that after 1 h of H_2O_2 treatment, ROS production linearly increased in a dose and time dependent manner (Figure S7).

As shown in Figure 7, all the compounds were able to significantly prevent ROS formation. Notably is that this effect was evident already at the lower tested doses (0.1, 0.5 and 1 μM), demonstrating a good protection towards oxidative damage. This efficacy at lower doses may be due to the synergism obtained by inhibition of both enzymes. It is possible to assume, that the lack of dose linearity is due to the fact that the protective mechanism induced by these compounds reaches its maximum effect already at the lower dose (0.1 μM) confirming the high efficacy of the compounds.

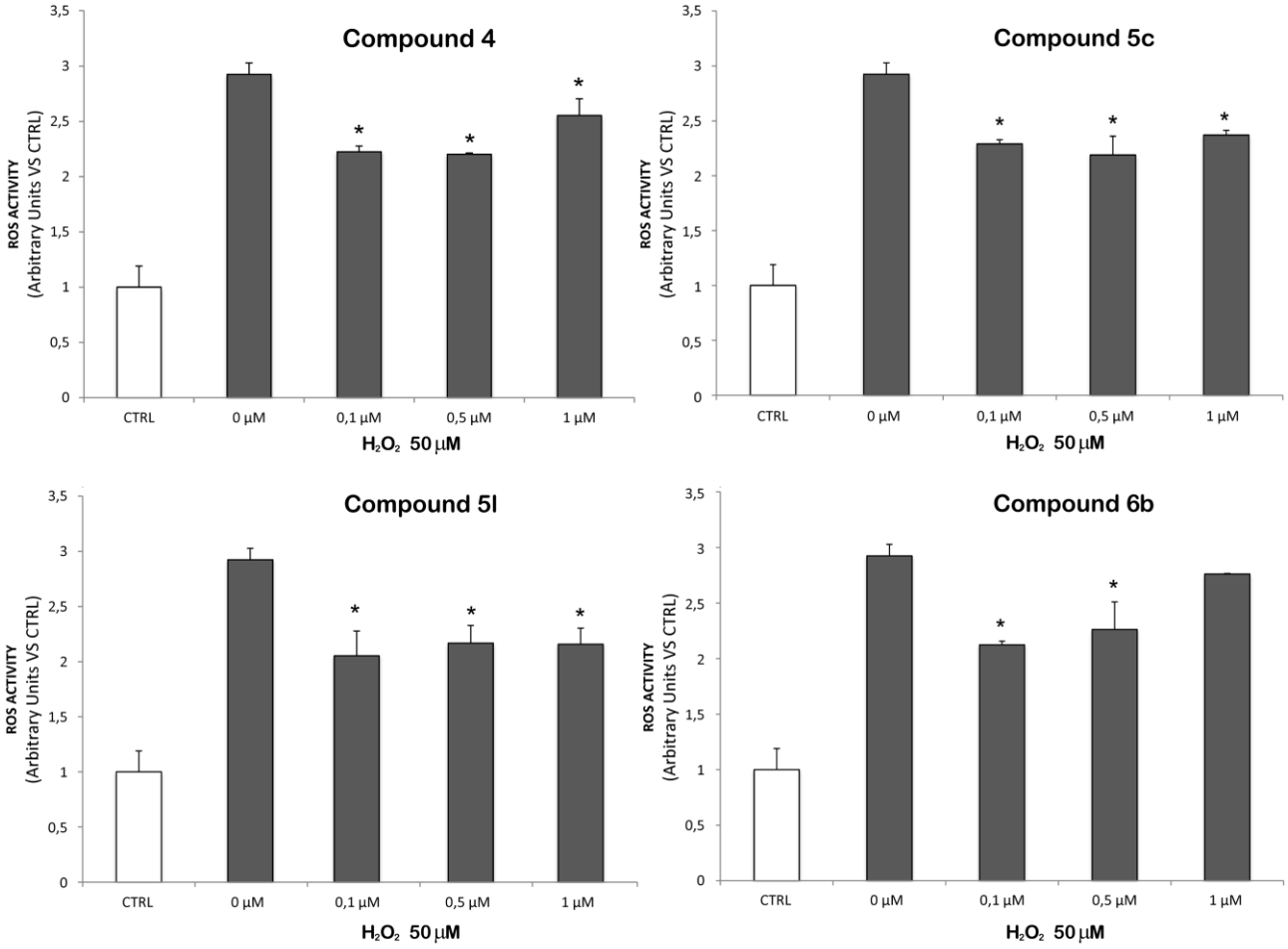

Figure 7. Prevention of ROS formation by the selected compounds (**4**, **5c**,**l** and **6b**). Values represent average ± SD for three experiments in triplicate. *$p < 0.05$ versus untreated sample (0 µM).

Based on these encouraging data, similar tests were performed in neuronal IMR 32 differentiated cells by a 12 days treatment with bromodeoxyuridine (BrdU). As shown in Figure 8, all the compounds were able to significantly prevent ROS production at very low doses (0.1-0.5 and 1 µM) after 50 µM H_2O_2 treatment. These outcomes, which demonstrated the good efficiency of the compounds **4**, **5c**, **5l**, and **6b** in preventing ROS formation also in differentiated neuronal cells, indicate these compounds as a possible new therapeutic strategy to prevent oxidative stress damage in neurodegenerative pathologies.

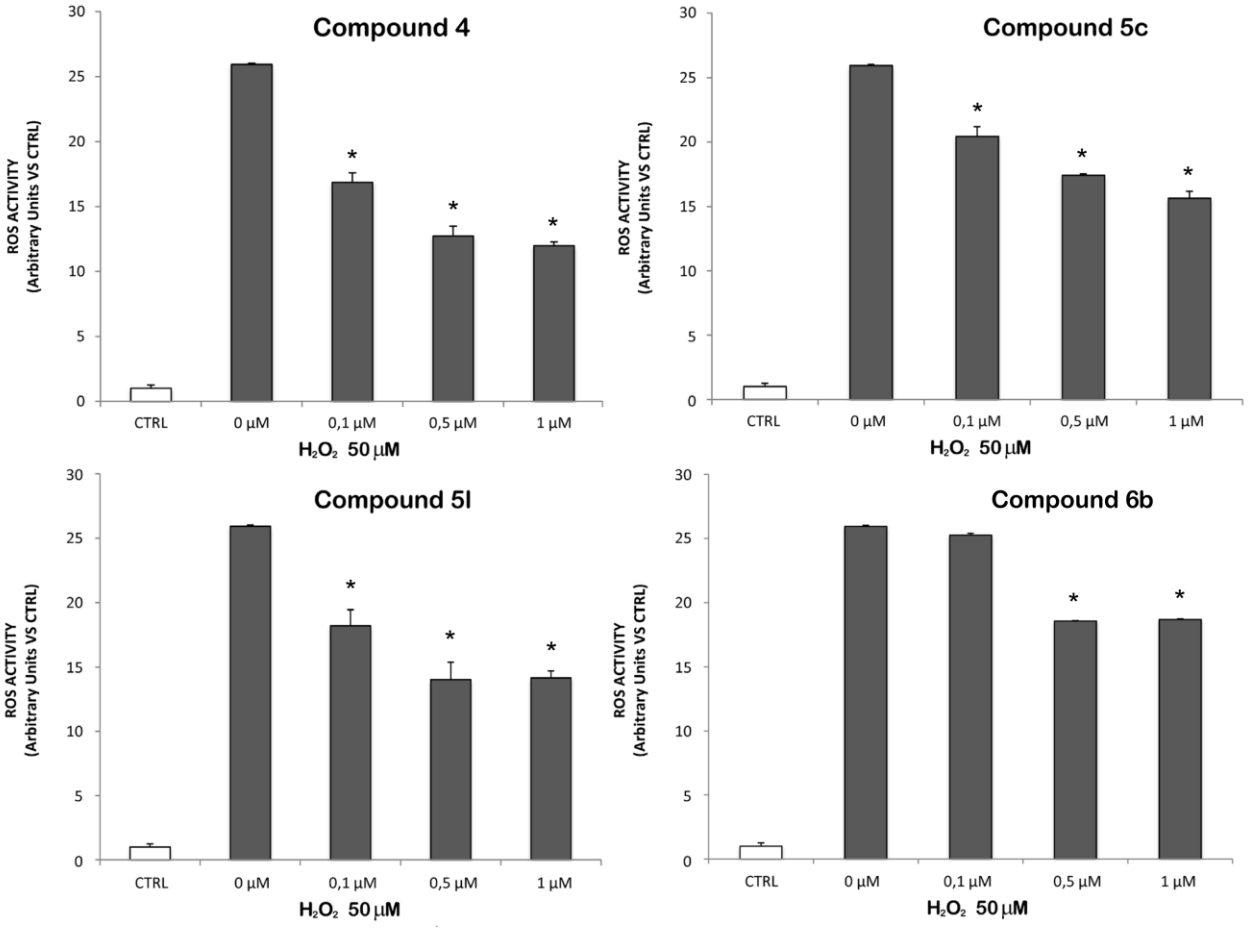

Figure 8. Compounds **4**, **5c**,**l** and **6b** prevent ROS formation (DCFDA Assay). Values represent average ± SD for three experiments in triplicate. *$p < 0.05$ versus untreated sample (0 µM).

3. Conclusion

In summary, we have described herein the rational design of the first MTDL prototypes for dual inhibition of *h*AK/*h*GSK-3β reported to date. For the most promising compounds of the series (**4**, **5c**,**l** and **6b**) their ability to counteract OS in neuronal cells was also experimentally measured. The described medicinal chemistry approach led to a novel series of compounds sharing the pharmacophoric requirements for interacting with both allosteric sites of the *h*AK/*h*GSK-3β enzymes. Non-competitive mechanism of action was ascertained for **5c** and **5l** in *h*GSK-3β. Subsequently, the most interesting dual *h*AK/*h*GSK-3β inhibitors (**4**, **5c**,**l** and **6b**) proved to be devoid of cytotoxicity towards the neuroblastoma

cell line IMR 32 and were engaged in biological assays to evaluate their ability to counteract ROS formation. Among the tested compounds, compound **5l** stood out as a good MTDL potentially endowed with therapeutic potential for neurodegenerative diseases. In fact **5l**, one of the best dual *h*AK/*h*GSK-3β inhibitors of the series, is able to counteract OS and preventing ROS formation in neuronal cells devoid of any cytotoxicity. The dual *h*AK/*h*GSK-3β inhibition approach herein described may lead to the development of innovative antioxidant/neuroprotective agents potentially useful for the treatment of neurological disorders.

4. Methods

4.1. Chemistry

4.1.1. General Procedures

Melting points were taken on a Gallenkamp melting point apparatus and are uncorrected. ^{1}H and ^{13}C NMR spectra were recorded on a Bruker Avance 300 MHz, a Varian 300 MHz, or a Bruker 400 MHz spectrometer. Splitting patterns are described as singlet (s), doublet (d), triplet (t), quartet (q), quintuplet (qt), and broad (br). Chromatographic separations were performed on silica gel (Kieselgel 40, 0.040-0.063 mm, Merck). Reactions and products mixtures were routinely monitored by thin-layer chromatography (TLC) on Merck 0.2 mm precoated silica (60 F254) aluminum sheets, with visualization by irradiation with a UV lamp. ESIMS and HRESIMS were carried out by a Thermo Finningan LCQ Deca XP Max ion-trap mass spectrometer equipped with Xcalibur software, and an LTQ Orbitrap XL mass spectrometer (Thermo FisherScientific, San Jose, CA, USA) operated in positive ion mode, respectively. The Orbitrap mass analyzer was calibrated according to the manufacturer's directions using a mixture of caffeine, methionine-arginine-phenylalanine-alanine-acetate (MRFA), and Ultramark 1621

in a solution of acetonitrile, methanol, and acetic acid. Data were collected and analyzed using the software provided by the manufacturer.

Structure of compounds **5a-g** was confirmed by Heteronuclear Multiple Bond Correlation (HMBC) experiments (400 MHz, Bruker Ascend^{TM} 400 spectrometer), and representative examples (**5a-d,f**) are reported in Supporting Information. All final compounds meet the criteria of > 95% purity, as confirmed by HRESIMS analysis. Yields refer to purified products and are not optimized. All starting materials, reagents and solvents (reagent grade) were purchased from Sigma-Aldrich and used without further purification.

*4.1.2. (±) 2-Naphthalen-1-yl-4H-benzo[1,4]oxazin-3-one (**9a**)*

A mixture of 2-aminophenol **7** (1.00 g, 9.16 mmol), bromonaphthalen-1-yl acetic acid methyl ester **8a** (3.07 g, 11.00 mmol), and K_2CO_3 (6.33 g, 45.80 mmol) in dry DMF (15 mL) was stirred at 100 °C for 5 h. The solvent was removed under reduced pressure, and the residue was taken up in EtOAc, and washed successively with 2M HCl, and brine. The organic phase was dried (Na_2SO_4), filtered, and concentrated under reduced pressure. The residue was purified by column chromatography (SiO_2, EtOAc/petroleum ether, 40−60 °C, 3:7 v/v, as eluent) to give the title compound as white solid (1.59 g, yield 63%); mp: 234-236 °C; ^{1}H NMR (300 MHz, DMSO-d_6) δ: 6.38 (s, 1H), 6.85-6.91 (m, 2H), 6.97-7.03 (m, 2H), 7.49 (d, 2H, J = 5.2 Hz), 7.59 (qt, 2H, J = 7.9 Hz), 7.97-8.00 (m, 2H), 8.24 (d, 1H, J = 8.3 Hz), 11.07 (s, 1H); ^{13}C NMR (75 MHz, DMSO-d_6) δ: 77.2, 116.2, 117.0, 123.1, 123.7, 125.00, 125.5, 126.5, 127.0, 127.3, 127.9, 129.1, 130.2, 131.6, 131.9, 134.1, 143.2, 166.0. ESI-MS *m/z* 276.1 $[M+H]^+$.

*4.1.3. (±) 2-Naphthalen-2-yl-4H-benzo[1,4]oxazin-3-one (**9b**)*

The title compound was obtained, according to the procedure described for **9a** using bromonaphthalen-2-yl acetic acid methyl ester **8b**, as a white solid (yield: 61%); mp: 171-173 °C; ^{1}H NMR (300 MHz, $CDCl_3$) δ: 5.89 (s, 1H), 6.83 (d, 1H, J = 7.3 Hz), 6.92-7.03 (m, 2H), 7.09 (d, 1H, J = 7.7 Hz), 7.49 (m, 2H), 7.61 (d, 1H, J = 8.4 Hz), 7.82-7.91 (m, 4H), 8.73 (brs, 1H); ^{13}C NMR (75 MHz, $CDCl_3$) δ: 78.8,

115.8, 117.4, 122.8, 124.4, 124.5, 125.9, 126.4, 126.5, 126.6, 127.7, 128.3, 128.7, 132.3, 133.0, 133.4, 142.9, 165.9. ESI-MS *m/z* 298.1 $[M+Na]^+$.

*4.1.4. (±) 2-Naphthalen-1-yl-3,4-dihydro-2H-benzo[1,4]oxazine (**10**)*

A solution of (±) 2-naphthalen-1-yl-4H-benzo[1,4]oxazin-3-one **9a** (0.743 g, 2.70 mmol) in dry THF (25 mL) was cooled to 0 °C, and then 7.0 mL of 2M in THF borane dimethyl sulfide complex (BH_3SMe_2) solution (1.06 g, 14.00 mmol) were added. The reaction mixture was stirred at rt for 12 h, then was cooled to 0 °C, and to it was slowly added 1N HCl until gas evolution ceased. The solvent was removed under reduced pressure, and the residue was taken up in EtOAc, and washed with saturated solution of $NaHCO_3$, and brine. The organic phase was dried (Na_2SO_4), filtered, and concentrated under reduced pressure. The residue was purified by column chromatography (SiO_2, EtOAc/petroleum ether, 40−60 °C, 3:7 v/v, as eluent) to give the title compound as white solid (0.628 g, yield 89%); mp: 129-131 °C; ^{1}H NMR (300 MHz, $CDCl_3$) δ: 3.52 (m, 1H), 3.76 (m, 1H), 4.01 (brs, 1H), 5.88 (d, 1H, *J* = 8.5 Hz), 6.77 (m, 2H), 6.88 (m, 1H), 7.00 (d, 1H, *J* = 7.7 Hz), 7.55 (m, 3H), 7.73 (d, 1H, *J* = 7.1 Hz), 7.86-7.94 (m, 2H), 8.09 (d, 1H, *J* = 8.6 Hz); ^{13}C NMR (75 MHz, $CDCl_3$) δ: 47.3, 73.3, 115.7, 117.3, 119.1, 121.6, 122.8, 124.1, 125.6, 125.7, 126.5, 128.7, 129.1, 130.3, 133.2, 133.7, 134.4, 144.8. ESI-MS *m/z* 262.1 $[M+H]^+$.

*4.1.5. (±) (5-Fluoro-2-nitrophenoxy)naphthalen-1-yl-acetic acid methyl ester (**12a**)*

To a solution of 5-fluoro-2-nitrophenol **11a** (0.300 g, 1.91 mmol) in dry DMF (5 mL) were added K_2CO_3 (1.32 g, 9.55 mmol), and bromonaphthalen-1-yl-acetic acid methyl ester **8a** (0.642 g, 2.30 mmol), and the resulting mixture was stirred at rt for 12 h. The solvent was removed under reduced pressure, and the residue was taken up in EtOAc, and washed with 2M HCl and brine. The organic phase was dried (Na_2SO_4), filtered, and concentrated under reduced pressure. The residue was purified by column chromatography (SiO_2, EtOAc/petroleum ether, 40−60 °C, 3:7 v/v, as eluent) to give the title compound as yellow solid (0.611 g, yield 90%); mp: 170-172 °C; ^{1}H NMR (300 MHz, $CDCl_3$) δ: 3.75 (s, 3H), 6.38

(s, 1H), 6.79 (m, 2H), 7.52-7.68 (m, 3H), 7.86-8.04 (m, 4H), 8.34 (d, 1H, J = 8.6 Hz); ^{13}C NMR (75 MHz, $CDCl_3$) δ: 53.2, 78.4, 103.8 (d, J_{C-F} = 26.9 Hz), 108.9 (d, J_{C-F} = 23.4 Hz), 123.5, 125.5, 126.3, 127.0, 127.2, 128.4 (d, J_{C-F} = 11.3 Hz), 129.0, 129.4, 130.3, 130.4, 133.9, 136.9, 152.7 (d, J_{C-F} = 11.2 Hz), 163.3 (d, J_{C-F} = 256.9 Hz), 168.7. ESI-MS *m/z* 378.1 $[M+Na]^+$.

*4.1.6. (±) (5-Morpholin-4-yl-2-nitrophenoxy) naphthalen-1-yl-acetic acid methyl ester (**12b**)*

The title compound was obtained according to the procedure described for **12a** using 5-morpholin-4-yl-2-nitrophenol **11b** [50]. Yellow solid; yield: 67%; mp: 200-202 °C; ^{1}H NMR (300 MHz, $CDCl_3$) δ: 3.11 (t, 4H, J = 4.9 Hz), 3.74 (m, 7H), 6.27 (s, 1H), 6.41-6.47 (m, 2H), 7.52-7.64 (m, 3H), 7.90-7.97 (m, 3H), 8.03 (d, 1H, J = 9.3 Hz), 8.39 (d, 1H, J = 8.5 Hz); ^{13}C NMR (75 MHz, $CDCl_3$) δ: 46.9, 53.0, 66.2, 78.4, 101.3, 106.8, 123.4, 125.7, 126.1, 127.0, 128.8, 129.0, 130.0, 130.4, 130.5, 131.0, 133.8, 153.3, 154.9, 155.2, 169.5. ESI-MS *m/z* 445.2 $[M+Na]^+$.

*4.1.7. (±) Naphthalen-1-yl-(6-nitrobenzo[1,3]dioxol-5-yloxy)acetic acid methyl ester(**12c**)*

The title compound was obtained, according to the procedure described for **12a** using 6-nitrobenzo[1,3]dioxol-5-ol **11c**, as a yellow solid (yield 87%); mp: 123-125 °C; ^{1}H NMR (300 MHz, $CDCl_3$) δ: 3.73 (s, 3H), 6.04 (m, 2H), 6.28 (s, 1H), 6.52 (s, 1H), 7.49-7.65 (m, 4H), 7.85 (d, 1H, J = 7.1 Hz), 7.92 (d, 2H, J = 8.0 Hz), 8.35 (d, 1H, J = 8.4 Hz); ^{13}C NMR (75 MHz, $CDCl_3$) δ: 53.0, 80.1, 99.3, 103.0, 105.9, 123.7, 125.4, 126.2, 127.1, 127.3, 129.0, 130.1, 130.2, 130.5, 133.9, 134.5, 142.4, 148.8, 152.5, 169.3. ESI-MS *m/z* 403.9 $[M+Na]^+$.

*4.1.8. (±) Naphthalen-2-yl-(6-nitrobenzo[1,3]dioxol-5-yloxy)acetic acid methyl ester (**12d**)*

The title compound was obtained, according to the procedure described for **12a** using 6-nitrobenzo[1,3]dioxol-5-ol **11c** and bromonaphthalen-2-yl-acetic acid methyl ester **8b**, as a pale yellow solid (yield 68%); mp: 141-144 °C; ^{1}H NMR (300 MHz, $CDCl_3$) δ: 3.76 (s, 3H), 5.82 (s, 1H), 6.07 (m, 2H), 6.57 (s, 1H), 7.52-7.57 (m, 3H), 7.74 (d, 1H, J = 8.5 Hz), 7.86-7.94 (m, 3H), 8.09 (s, 1H); ^{13}C NMR

(75 MHz, $CDCl_3$) δ: 53.0, 81.5, 99.1, 103.1, 106.0, 124.1, 126.6, 126.9, 127.1, 127.8, 128.4, 129.0, 131.5, 133.1, 133.7, 134.3, 142.4, 148.8, 152.6, 169.3. ESI-MS *m/z* 404.3 $[M+Na]^+$.

*4.1.9. (±) (6-Nitrobenzo[1,3]dioxol-5-yloxy)phenyl-acetic acid methyl ester (**12e**)*

The title compound was obtained, according to the procedure described for **12a** using 6-nitrobenzo[1,3]dioxol-5-ol **11c** and 2-bromo-2-phenylacetic acid methyl ester **8c**, as yellow solid (yield 75%); ^1H NMR (300 MHz, $CDCl_3$) δ: 3.75 (s, 3H), 5.66 (s, 1H), 6.08 (s, 2H), 6.53 (s, 1H), 7.43 (m, 3H), 7.50 (s, 1H), 7.62 (d, 2H, *J* = 5.9 Hz); ^{13}C NMR (75 MHz, $CDCl_3$) δ: 53.0, 81.3, 98.8, 103.0, 106.0, 127.2, 128.9, 129.4, 134.1, 134.2, 142.3, 148.8, 152.6, 169.3. ESI-MS *m/z* 354.1 $[M+Na]^+$.

*4.1.10. (±) 7-Fluoro-2-naphthalen-1-yl-4H-benzo[1,4]oxazin-3-one (**13a**)*

To a solution of **12a** (0.400 g, 1.13 mmol) in THF (25 mL), water (25 mL) and saturated solution of NH_4Cl (30 mL) was added iron powder (0.631 g, 11.30 mmol), and the reaction mixture was stirred at 100 °C for 3 h. After cooling to rt, the volatiles were removed under reduced pressure, and the residue was diluted with EtOAc, and filtered through a small pad of celite. The filtrate was successively washed with water, and saturated aqueous solution of $NaHCO_3$ (40 mL). The organic phase was dried over dry Na_2SO_4, filtered, and concentrated under reduced pressure. The residue was purified by column chromatography (SiO_2, EtOAc/petroleum ether, 40−60 °C, 3:7 v/v, as eluent) to give the title compound as white solid (0.268 g, yield 81%); mp: 206-207 °C; ^1H NMR (300 MHz, $CDCl_3$) δ: 6.32 (s, 1H), 6.57-6.73 (m, 3H), 7.40-7.50 (m, 2H), 7.60 (qt, 2H, *J* = 7.9 Hz), 7.92 (d, 2H, *J* = 6.9 Hz), 8.27 (d, 1H, *J* = 8.2 Hz), 9.72 (brs, 1H); ^{13}C NMR (75 MHz, $CDCl_3$) δ: 77.3, 105.4 (d, $J_{C\text{-}F}$ = 26.2 Hz), 109,4 (d, $J_{C\text{-}F}$ = 23.2 Hz), 116.4 (d, $J_{C\text{-}F}$ = 9.7 Hz), 122.6 (d, $J_{C\text{-}F}$ = 2.9 Hz), 124.0, 124.9, 126.2, 126.4, 126.9, 129.0, 129.8, 130.6, 131.4, 134.2, 143.7 (d, $J_{C\text{-}F}$ = 12.1 Hz), 159.2 (d, $J_{C\text{-}F}$ = 243.2 Hz), 166.5. ESI-MS *m/z* 316.1 $[M+Na]^+$.

*4.1.11. (±) 7-Morpholin-4-yl-2-naphthalen-1-yl-4H-benzo[1,4]oxazin-3-one (**13b**)*

The title compound was obtained according to the procedure described for **13a** using (±) (5-morpholin-4-yl-2-nitrophenoxy)naphthalen-1-yl-acetic acid methyl ester **12b** (0.300 g, 0.710 mmol). After purification by column chromatography (SiO_2, EtOAc/petroleum ether, 40−60 °C, 3:7 v/v, as eluent) the title compound was obtained as white solid (0.187 g, yield 73%); mp: 263-264 °C; ^{1}H NMR (300 MHz, $CDCl_3$) δ: 3.02 (t, 4H, *J* = 4.5 Hz), 3.79 (t, 4H, *J* = 4.5 Hz), 6.30 (s, 1H), 6.48 (m, 2H), 6.77 (d, 1H, *J* = 8.4 Hz), 7.38-7.63 (m, 4H), 7.89 (m, 2H), 8.28 (d, 1H, *J* = 8.3 Hz), 8.96 (brs, 1H); ^{13}C NMR (75 MHz, $CDCl_3$) δ: 49.5, 66.8, 77.5, 105.3, 110.0, 116.1, 119.1, 124.2, 125.0, 126.0, 126.4, 126.8, 128.9, 130.3, 130.3, 131.5, 134.2, 143.8, 148.7, 165.7. ESI-MS *m/z* 361.2 $[M+H]^+$.

*4.1.12. (±) 6-Naphthalen-1-yl-8H-1,3,5-trioxa-8-azacyclopenta[b]naphthalen-7-one (**13c**)*

To a solution of (±) naphthalen-1-yl-(6-nitrobenzo[1,3]dioxol-5-yloxy)acetic acid methyl ester **12c** (1.20 g, 3.15 mmol) in EtOH (15 mL) was added $SnCl_2$ (2.99 g, 15.75 mmol and the resulting mixture was stirred at 80 °C for 12 h. Then the solvent was removed under reduced pressure, and the residue was taken up in EtOAc, and washed with 1N HCl, 1N NaOH and brine. The organic phase was dried (Na_2SO_4), filtered, and evaporated under vacuo. After work up, the compound was used in the next step without further purification. Crystallization of an analytical sample by EtOAc/*n*-hexane gave pure compound as white solid (0.764 g, yield 76%); mp: 249-251 °C; ^{1}H NMR (300 MHz, $CDCl_3$) δ: 5.88 (d, 2H, *J* = 10.6 Hz), 6.21 (s, 1H), 6.43 (d, 2H, *J* = 4.9 Hz), 7.39-7.48 (m, 2H), 7.52-7.63 (m, 2H), 7.90 (m, 2H), 8.05 (brs, 1H), 8.27 (d, 1H, *J* = 8.5 Hz); ^{13}C NMR (75 MHz, $CDCl_3$) δ: 97.0, 100.0, 101.5, 119.7, 124.2, 124.9, 126.1, 126.3, 126.8, 128.9, 129.8, 130.4, 131.5, 134.13, 137.4, 143.0, 143.8, 166.1. ESI-MS *m/z* 320.5 $[M+H]^+$.

*4.1.13. (±) 6-Naphthalen-2-yl-8H-1,3,5-trioxa-8-azacyclopenta[b]naphthalen-7-one (**13d**)*

The title compound was obtained according to the procedure described for **13c** using naphthalen-2-yl-(6-nitrobenzo[1,3]dioxol-5-yloxy)acetic acid methyl ester **12d** (0.900 g, 2.36 mmol). After work up, the compound was used in the next step without further purification. Crystallization of an analytical sample

by EtOAc/*n*-hexane gave pure compound as white solid (0.595 g, yield 79%); ^{1}H NMR (300 MHz, $CDCl_3$) δ: 5.79 (s, 1H), 5.88 (d, 2H, *J* = 10.3 Hz), 6.38 (s, 1H), 6.64 (s, 1H), 7.48-7.51 (m, 2H), 7.59 (d, 1H, *J* = 8.5 Hz), 7.82.-7.88 (m, 4H), 8.52 (brs, 1H); ^{13}C NMR (75 MHz, $CDCl_3$) δ: 78.7, 97.2, 99.9, 101.5, 119.3, 124.4, 126.4, 126.5, 126.6, 127.7, 128.3, 128.7, 131.9, 132.9, 133.4, 137.2, 143.0, 144.0, 165.6. ESI-MS *m/z* 342.1 $[M+Na]^+$.

*4.1.14. (±) 6-Phenyl-8H-1,3,5-trioxa-8-azacyclopenta[b]naphthalen-7-one (**13e**)*

The title compound was obtained according to the procedure described for **13c** using (6-nitrobenzo[1,3]dioxol-5-yloxy)phenylacetic acid methyl ester **12e** (0.230 g, 0.694 mmol). After purification by column chromatography (SiO_2, EtOAc/petroleum ether, 40−60 °C, 3:7 v/v, as eluent) the title compound was obtained as white solid (0.162 g, yield 87%); mp: 222-225 °C; ^{1}H NMR (300 MHz, $CDCl_3$) δ: 5.62 (s, 1H), 5.92 (dd, 2H, *J* = 5.7, 1.3 Hz), 6.35 (s, 1H), 6.62 (s, 1H), 7.36-7.47 (m, 5H), 8.07 (brs, 1H); ^{13}C NMR (75 MHz, $CDCl_3$) δ: 78.4, 97.3, 99.7, 101.4, 119.2, 127.0, 128.7, 128.9, 134.7, 137.1, 142.8, 143.9, 166.1. ESI-MS *m/z* 292.1 $[M+Na]^+$.

*4.1.15. Acetic acid benzo[1,3]dioxol-5-ylester (**15**)*

To a stirred solution of benzo[1,3]dioxol-5-ol **14** (2.00 g, 14.48 mmol) in 10% w/v NaOH (20 mL, 2.00 g, 50.00 mmol) at 0 °C, acetic anhydride (7.39 g, 72.40 mmol) was added. Then, when no starting material was detected by TLC (DCM as eluent), the reaction mixture was extracted with DCM. The organic phase was washed with a saturated solution of $NaHCO_3$ and brine, then was dried on dry Na_2SO_4, filtered, and concentrated under reduced pressure. The title compound was obtained as a colorless liquid (2.53 g, yield 97%), and was used in the next step without further purification. ^{1}H NMR (300 MHz, $CDCl_3$) δ: 2.28 (s, 3H), 6.00 (s, 2H), 6.54 (dd, 1H, *J* = 8.4, 2.4 Hz), 6.62 (d, 1H, *J* = 2.4 Hz), 6.78 (d, 1H, *J* = 8.4 Hz).

*4.1.16. Acetic acid 6-nitrobenzo[1,3]dioxol-5-ylester (**16**)*

Acetic acid benzo[1,3]dioxol-5-yl ester **15** (2.51 g, 13.93 mmol) was dissolved in glacial acetic acid (5 mL), then a solution of concentrated HNO_3 1.1 mL (70%, d = 1.413, 1.09 g, 17.27 mmol) in glacial acetic acid (2 mL) was added dropwise. The reaction mixture was stirred at rt for 4 h, then was cooled at 0 °C. The yellow solid was filtrated, washed with cold water, air-dried, and used in the next step without further purification (2.95 g, yield 94%). ^{1}H NMR (300 MHz, $CDCl_3$) δ: 2.37 (s, 3H), 6.15 (s, 2H), 6.65 (s, 1H), 7.60 (s, 1H).

*4.1.17. 6-Nitrobenzo[1,3]dioxol-5-ol (**11c**)*

A solution of acetic acid 6-nitrobenzo[1,3]dioxol-5-yl ester **16** (2.80 g, 12.44 mmol) in 20% H_2SO_4 (30 mL) was heated at 80 °C until no starting material was detected by TLC (DCM as eluent). After cooling at rt, the reaction mixture was poured over crushed ice, and after 1 h the yellow precipitate was filtrated, air-dried, and used in the next step without further purification (2.05 g, yield 90%); ^{1}H NMR (300 MHz, $CDCl_3$) δ: 6.11 (s, 2H), 6.59 (s, 1H), 7.49 (s, 1H), 11.41 (s, 1H); ^{13}C NMR (75 MHz, $CDCl_3$) δ: 98.8, 102.4, 103.0, 141.8, 155.7, 156.3.

*4.1.18. 3-Hydroxy-3-(p-tolyl)indolin-2-one (**18a**)*

To a solution of isatin **17** (500 mg, 3.40 mmol) in 15 mL of dry THF at -15 °C NaH (60% dispersion in mineral oil, 204.00 mg, 5.10 mmol) was added. The mixture was kept under stirring at -15 °C for 30 min after which of *p*-tolylmagnesium bromide (1 M solution in THF, 10.2 mL) was added. The mixture was allowed to warm up to rt and then it was neutralized with 10 mL of a saturated solution of NH_4Cl. The aqueous phase was extracted with diethyl ether (3 x 15 mL). The combined organic phases were washed with brine (20 mL), dried over anhydrous Na_2SO_4, filtered and concentrated. The crude product was recrystallized in petroleum ether (2 x 3 mL) to give a light orange solid, which was subjected to the next step without further purification (yield 71%). ESI-MS *m/z* 261.9 $[M+Na]^+$.

*4.1.19. 3-Hydroxy-3-(naphthalen-1-yl)indolin-2-one (**18b**)*

Title compound was obtained following the procedure described for **18a** and using 1-naphthylmagnesium bromide as an orange solid (yield 75%). ESI-MS *m/z* 297.9 $[M+Na]^+$, 672.9 $[2M+Na]^+$.

*4.1.20. 3-(p-Tolyl)indolin-2-one (**19a**)*

$SnCl_2$ (3.015 g, 15.90 mmol) was added, at rt, to a stirred solution of compound **18a** (1.900 g, 7.95 mmol) in 48 mL of AcOH and 3.2 mL of HCl. The mixture was kept under stirring at 115 °C for 2.5 h and then allowed to cool to rt. After adding water (15 mL), the reaction mixture was extracted with EtOAc (50 mL) and the organic phase was washed with a saturated solution of Na_2CO_3 (2 x 50 mL) and with brine (50 mL), dried over anhydrous Na_2SO_4, filtered and concentrated. The crude product was recrystallized in petroleum ether (2 x 3 mL) to give a dark orange solid, which was subjected to the next step without further purification (yield 56%). ESI-MS *m/z* 245.9 $[M+Na]^+$.

*4.1.21. 3-(Naphthalen-1-yl)indolin-2-one (**19b**)*

Title compound was obtained, starting from compound **18b** and 1-naphthylmagnesium bromide, following the procedure reported for compound **19a**, as a dark orange solid (yield 95%).

*4.1.22. (±) 4-Benzyl-2-naphthalen-1-yl-4H-benzo[1,4]oxazin-3-one (**5a**)*

To a solution of *(±)* 2-naphthalen-1-yl-4H-benzo[1,4]oxazin-3-one **9a** (0.200 g, 0.726 mmol) in dry DMF (4 mL) Cs_2CO_3 (0.710 g, 2.18 mmol) and benzyl bromide (0.150 g, 0.877 mmol) were added, and the resulting mixture was stirred at rt for 12 h. The solvent was removed under vacuum, and the residue was taken up in DCM and washed with 1N HCl and brine. The organic phase was dried (Na_2SO_4), filtered, and evaporated in vacuo. The residue was purified by column chromatography (SiO_2, EtOAc/petroleum ether, 40−60 °C, 4:1 v/v, as eluent), to give after recrystallization (EtOAc/*n*-hexane) the title compound as white solid (0.151 g, yield 57%); mp: 118-120 °C; ^{1}H NMR (300 MHz, $CDCl_3$) δ: 5.34 (m, 2H), 6.42 (s, 1H), 6.91-6.98 (m, 3H), 7.07 (d, 1H, J = 7.00 Hz), 7.30-7.46 (m, 7H), 7.54-7.63 (m, 2H), 7.89 (t, 2H, J = 9.1 Hz), 8.32 (d, 1H, J = 8.4 Hz); ^{13}C NMR (75 MHz, $CDCl_3$) δ: 45.6, 77.6, 115.5, 117.7, 122.8,

124.1, 124.3, 124.8, 126.0, 126.3, 126.69, 127.3, 127.6, 128.9, 128.9, 129.0, 130.2, 130.8, 131.6, 134.2, 136.3, 144.4, 165.5. HRMS (ESI) *m/z* 366.1481 $[M+H]^+$ (calcd. for $[C_{25}H_{20}NO_2]^+$, 366.1494).

*4.1.23. (±) 4-(4-Methyl-benzyl)-2-naphthalen-1-yl-4H-benzo[1,4]oxazin-3-one (**5b**)*

Following the same procedure described for **5a** and starting from **9a** (0.300 g, 1.09 mmol) and 4-methylbenzyl bromide (0.242 g, 1.31 mmol), the title compound was obtained as white solid (0.223 g, yield 54%); mp: 133-135 °C; ^{1}H NMR (300 MHz, $CDCl_3$) δ: 2.36 (s, 3H), 5.29 (s, 2H), 6.40 (s, 1H), 6.91 (m, 3H), 7.01 (d, 1H, J = 6.8 Hz), 7.14 (d, 2H, J = 7.7 Hz), 7.31-7.45 (m, 4H), 7.58 (qt, 2H, J = 7.9 Hz), 7.89 (t, 2H, J = 7.9 Hz), 8.31 (d, 1H, J = 8.2 Hz); ^{13}C NMR (75 MHz, $CDCl_3$) δ: 21.1, 45.3, 77.6, 115.5, 117.6, 122.7, 124.0, 124.3, 124.8, 126.0, 126.3, 126.6, 127.2, 128.8, 129.0, 129.5, 130.1, 130.7, 131.5, 133.3, 134.1, 137.3, 144.3, 165.4. HRMS (ESI) *m/z* 380.1636 $[M+H]^+$ (calcd. for $[C_{26}H_{22}NO_2]^+$, 380.1650).

*4.1.24. (±) 4-(4-Fluorobenzyl)-2-naphthalen-1-yl-4H-benzo[1,4]oxazin-3-one (**5c**)*

Following the same procedure described for **5a**, and starting from **9a** (0.270 g, 0.981 mmol) and 4-fluorobenzyl bromide (0.223 g, 1.18 mmol), the title compound was obtained as white solid (0.256 g, yield 68%); mp: 136-138 °C; ^{1}H NMR (300 MHz, $CDCl_3$) δ: 5.30 (m, 2H), 6.39 (s, 1H), 6.91-6.97 (m, 3H), 7.04-7.10 (m, 3H), 7.38-7.42 (m, 4H), 7.58 (qt, 2H, J = 7.6 Hz), 7.89 (t, 2H, J = 7.2 Hz), 8.29 (d, 1H, J = 8.2 Hz); ^{13}C NMR (75 MHz, $CDCl_3$) δ: 44.8, 77.6, 115.3, 115.8 (d, $J_{C\text{-}F}$ = 21.6 Hz), 117.7, 122.8, 124.2, 124.2, 124.8, 126.1, 126.2, 126.7, 128.7, 128.8, 129.0 (d, $J_{C\text{-}F}$ = 8.1 Hz), 130.2, 130.6, 131.4, 132.0 (d, $J_{C\text{-}F}$ = 3.1 Hz), 134.1, 144.3, 162.2 (d, $J_{C\text{-}F}$ = 246.1 Hz), 165.5. HRMS (ESI) *m/z* 384.1394 (calcd. for $[C_{25}H_{19}FNO_2]^+$, 384.1400).

*4.1.25. (±) 4-(4-Chloro-benzyl)-2-naphthalen-1-yl-4H-benzo[1,4]oxazin-3-one (**5d**)*

Following the same procedure described for **5a**, and starting from **9a** (0.240 g, 0.872 mmol) and 4-chlorobenzyl bromide (0.216 g, 1.05 mmol), the title compound was obtained as white solid (0.192 g, yield 55%); mp: 112-114 °C; ^{1}H NMR (300 MHz, $CDCl_3$) δ: 5.29 (m, 2H), 6.40 (s, 1H), 6.92-7.03 (m,

4H), 7.36-7.43 (m, 6H), 7.58 (qt, 2H, *J* = 7.5 Hz), 7.89 (t, 2H, *J* = 7.8 Hz), 8.28 (d, 1H, *J* = 8.2 Hz); ^{13}C NMR (75 MHz, $CDCl_3$) δ: 44.9, 77.6, 115.3, 117.8, 122.9, 124.2, 124.3, 124.8, 126.1, 126.3, 126.7, 128.7, 128.7, 128.9, 129.1, 130.3, 130.6, 131.5, 133.5, 134.1, 134.8, 144.4, 165.5. HRMS (ESI) *m/z* 400.1089 $[M+H]^+$ (calcd. for $[C_{25}H_{19}ClNO_2]^+$, 400.1104).

*4.1.26. (±) 2-Naphthalen-1-yl-4-(4-nitrobenzyl)-4H-benzo[1,4]oxazin-3-one (**5e**)*

Following the same procedure described for **5a**, and starting from **9a** (0.300 g, 1.09 mmol) and 4-nitrobenzyl bromide (0.283 g, 1.31 mmol), the title compound was obtained as white solid (0.273 g, yield 61%); mp: 152-153 °C; ^{1}H NMR (300 MHz, $CDCl_3$) δ: 5.32-5.51 (q, 2H, *J* = 16.4 Hz), 6.42 (s, 1H), 6.95 (m, 4H), 7.38-7.45 (m, 2H), 7.54-7.64 (m, 4H), 7.91 (m, 2H), 8.23-8.30 (m, 3H); ^{13}C NMR (75 MHz, $CDCl_3$) δ: 44.9, 77.6, 114.9, 118.0, 123.0, 124.1, 124.2, 124.6, 124.8, 126.1, 126.1, 126.7, 127.9, 128.4, 128.4, 128.9, 130.4, 131.4, 134.1, 143.7, 144.4, 147.4, 165.6. HRMS (ESI) *m/z* 411.1340 $[M+H]^+$ (calcd. for $[C_{25}H_{19}N_2O_4]^+$ 411.1345).

*4.1.27. (±) 4-(4-Methoxybenzyl)-2-naphthalen-1-yl-4H-benzo[1,4]oxazin-3-one (**5f**)*

Following the same procedure described for **5a**, and starting from **9a** (0.280 g, 1.02 mmol) and 4-methoxybenzyl bromide (0.246 g, 1.22 mmol), the title compound was obtained as white solid (0.258 g, 64%); mp: 132-133 °C; ^{1}H NMR (300 MHz, $CDCl_3$) δ: 3.82 (s, 3H), 5.27 (s, 2H), 6.38 (s, 1H), 6.87-6.99 (m, 5H), 7.10 (d, 1H, *J* = 7.2 Hz), 7.35-7.43 (m, 4H), 7.57 (qt, 2H, *J* = 7.6 Hz), 7.88 (t, 2H, *J* = 8.2 Hz), 8.30 (d, 1H, *J* = 8.1 Hz); ^{13}C NMR (75 MHz, $CDCl_3$) δ: 45.0, 55.3, 77.5, 114.2, 115.5, 117.6, 122.7, 124.0, 124.3, 124.8, 126.0, 126.3, 126.6, 128.4, 128.7, 128.8, 128.9, 130.1, 130.7, 131.5, 134.1, 144.3, 159.0, 165.4. HRMS (ESI) *m/z* 396.1577 $[M+H]^+$ (calcd. for $[C_{26}H_{22}NO_3]^+$, 396.1600).

*4.1.28. (±) 4-(4-Fluorobenzyl)-2-naphthalen-2-yl-4H-benzo[1,4]oxazin-3-one (**5g**)*

Following the same procedure described for **5a**, and starting from **9b** (0.250 g, 0.908 mmol) and 4-fluorobenzyl bromide (0.206 g, 1.09 mmol), the title compound was obtained as white solid (0.171 g, yield 49%); mp: 117-119 °C; ^{1}H NMR (300 MHz, $CDCl_3$) δ: 5.08 (d, 1H, *J* = 16.0 Hz), 5.37 (d, 1H, *J* =

16.0 Hz), 6.02 (s, 1H), 6.85-7.03 (m, 5H), 7.15 (d, 1H, J = 7.9 Hz), 7.24 (m, 2H), 7.50 (m, 2H), 7.62 (d, 1H, J = 9.0 Hz), 7.77-7.87 (m, 4H); ^{13}C NMR (75 MHz, $CDCl_3$) δ: 44.8, 78.6, 115.4, 115.8 (d, $J_{C\text{-}F}$ = 21.6 Hz), 117.9, 122.8, 124.2, 124.4, 126.2, 126.4, 126.6, 127.7, 128.2, 128.4, 128.4 (d, $J_{C\text{-}F}$ = 8.1 Hz), 128.7, 131.8 (d, $J_{C\text{-}F}$ = 3.2 Hz), 132.4, 132.9, 133.3, 144.1, 162.1 (d, $J_{C\text{-}F}$ = 245.9 Hz), 164.8. HRMS (ESI) *m/z* 384.1395 $[M+H]^+$ (calcd. for $[C_{25}H_{19}FNO_2]^+$ 384.1400).

*4.1.29. (±) 2-Naphthalen-1-yl-2,3-dihydro-benzo[1,4]oxazin-4-yl)phenyl-methanone (**5h**)*

To a cooled (0 °C) solution of **10** (0.300 g, 1.15 mmol) and triethylamine (0.233 g, 2.30 mmol) in dry DCM (5 mL), a solution of benzoyl chloride (0.242 g, 1.72 mmol) in dry DCM (3 mL) was added dropwise. The resulting reaction mixture was allowed to warm to rt, and stirred under these conditions for 12 h. Then the reaction mixture was washed with 1 N HCl, 1 N NaOH and brine. The organic phase was dried (Na_2SO_4), filtered and concentrated under vacuum. The residue was purified by column chromatography (SiO_2, EtOAc/petroleum ether, 40−60 °C, 4.5:0.5 v/v, as eluent) to give, after recrystallization (EtOAc/*n*-hexane), the title compound as white solid (0.155 mg, yield 37%); mp: 138-140 °C; ^{1}H NMR (300 MHz, $CDCl_3$) δ: 3.68-3.76 (dd, 2H, J = 13.5, 8.5 Hz), 4.74 (m, 1H), 6.08 (d, 2H, J = 7.7 Hz), 6.84 (m, 1H), 7.10-7.56 (m, 9H), 7.70 (d, 1H, J = 7.7 Hz), 7.81-7.92 (m, 3H); ^{13}C NMR (75 MHz, $CDCl_3$) δ: 47.9, 75.1, 117.4, 120.2, 122.0, 123.9, 124.6, 125.3, 125.8, 125.9, 126.7, 128.1, 128.4, 129.1, 129.1, 129.8, 130.6, 132.7, 133.7, 134.9, 146.9, 169.2. HRMS (ESI) *m/z* 366.1482 $[M+H]^+$ (calcd. for $[C_{25}H_{20}NO_2]^+$, 366.1494).

*4.1.30. (±) 4-Benzenesulfonyl-2-naphthalen-1-yl-3,4-dihydro-2H-benzo[1,4]oxazine (**5i**)*

Following the same procedure described for **5h**, and starting from **10** (0.220 g, 0.842 mmol) and benzenesulfonyl chloride (0.222 g, 1.26 mmol), the title compound was obtained as white solid (0.233 g, yield 69%); mp: 74-76 °C; ^{1}H NMR (300 MHz, $CDCl_3$) δ: 3.41 (dd, 1H, J = 14.7, 10.3 Hz), 4.59 (d, 1H, J = 14.7 Hz), 5.26 (d, 1H, J = 10.1 Hz), 7.07 (m, 2H), 7.20 (m, 1H), 7.48-7.67 (m, 8H), 7.83-7.98 (m, 5H); ^{13}C NMR (75 MHz, $CDCl_3$) δ: 49.5, 71.1, 117.9, 121.2, 122.3, 123.5, 124.2, 124.7, 125.5, 125.9,

126.6, 126.6, 127.5, 129.2, 129.3, 129.5, 130.0, 132.6, 133.6, 133.7, 139.1, 147.5. HRMS (ESI) *m/z* 402.1163 $[M+H]^+$ (calcd. for $[C_{24}H_{20}NO_3S]^+$ 402.1164).

*4.1.31. (±) 7-Fluoro-4-(4-fluorobenzyl)-2-naphthalen-1-yl-3,4-dihydro-2H-benzo[1,4]oxazine (**5j**)*

Following the same procedure described for **5a**, and starting from **13a** (0.240 g, 0.818 mmol) and 4-fluorobenzyl bromide (0.186 g, 0.982 mmol), the title compound was obtained as white solid (0.220 g, yield 67%); mp: 100-101 °C; ^{1}H NMR (300 MHz, $CDCl_3$) δ: 5.22-5.34 (m, 2H), 6.43 (s, 1H), 6.61-6.69 (m, 2H), 6.94-6.99 (m, 1H), 7.08 (m, 2H), 7.38 (m, 4H), 7.54-7.64 (m, 2H), 7.90 (m, 2H), 8.26 (d, 1H, J = 8.2 Hz); ^{13}C NMR (75 MHz, $CDCl_3$) δ: 45.0, 77.5, 105.9 (d, $J_{C\text{-}F}$= 25.9 Hz), 109.3 (d, $J_{C\text{-}F}$ = 22.8 Hz), 115.9 (d, $J_{C\text{-}F}$ = 9.7 Hz), 115.9 (d, $J_{C\text{-}F}$ = 21.6 Hz), 124.1, 124.8, 125.2 (d, $J_{C\text{-}F}$= 3.1 Hz), 126.1 (d, $J_{C\text{-}F}$= 6.3 Hz), 126.9, 128.8, 128.9, 129.1, 130.1, 130.5, 131.4, 131.8 (d, $J_{C\text{-}F}$= 3.2 Hz), 134.1, 145.2 (d, $J_{C\text{-}F}$= 11.9 Hz), 159.0 (d, $J_{C\text{-}F}$= 244.5 Hz), 162.3 (d, $J_{C\text{-}F}$= 247.0 Hz), 164.9. HRMS (ESI) *m/z* 402.1303 $[M+H]^+$ (calcd. for $[C_{25}H_{18}F_2NO_2]^+$ 402.1306).

*4.1.32. (±) 4-(4-Fluorobenzyl)-7-morpholin-4-yl-2-naphthalen-1-yl-4H-benzo[1,4]oxazin-3-one (**5k**)*

Following the same procedure described for **5a**, and starting from **13b** (0.230 g, 0.638 mmol) and 4-fluorobenzyl bromide (0.145 g, 0.767 mmol), the title compound was obtained as white solid (0.206 g, yield 69%); mp: 155-157 °C; ^{1}H NMR (300 MHz, $CDCl_3$) δ: 3.01 (t, 4H, J = 4.8 Hz), 3.78 (t, 4H, J = 4.8 Hz), 5.26 (q, 2H, J = 12.5 Hz), 6.38 (s, 1H), 6.49 (m, 2H), 6.94 (d, 1H, J = 9.0 Hz), 7.06 (t, 2H, J = 4.3 Hz), 7.35-7.41 (m, 4H), 7.58 (qt, 2H, J = 7.8 Hz), 7.89 (t, 2H, J = 8.7 Hz), 8.27 (d, 1H, J = 8.2 Hz); ^{13}C NMR (75 MHz, $CDCl_3$) δ: 44.7, 49.1, 66.7, 77.6, 105.3, 109.4, 115.8 (d, $J_{C\text{-}F}$ = 21.6 Hz), 115.3, 121.4, 124.2, 124.9, 126.0, 126.2, 126.7, 129.0 (d, $J_{C\text{-}F}$ = 11.8 Hz), 129.1, 130.2, 131.5, 132.2 (d, $J_{C\text{-}F}$ = 3.2 Hz), 134.2, 145.1, 148.3, 160.6, 163.8, 164.8. HRMS (ESI) *m/z* 469.1914 $[M+H]^+$ (calcd. for $[C_{29}H_{26}FN_2O_3]^+$ 469.1927).

*4.1.33. (±) 8-Benzyl-6-naphthalen-1-yl-8H-1,3,5-trioxa-8-azacyclopenta[b]naphthalen-7-one (**5l**)*

Following the same procedure described for **5a**, and starting from **13c** (0.200 g, 0.626 mmol) and benzyl bromide (0.130 g, 0.760 mmol), the title compound was obtained as white solid (0.197 g, yield 77%); mp: 174-176 °C; ^{1}H NMR (300 MHz, $CDCl_3$) δ: 5.28 (q, 2H, *J* = 26.2 Hz), 5.84 (d, 2H *J* = 11.9 Hz), 6.34 (s, 1H), 6.41 (s, 1H), 6.61 (s, 1H), 7.37-7.41 (m, 7H), 7.53-7.64 (m, 2H), 7.89 (t, 2H, *J* = 7.3 Hz), 8.30 (d, 1H, *J* = 8.3 Hz); ^{13}C NMR (75 MHz, $CDCl_3$) δ: 46.0, 77.7, 97.3, 100.0, 101.4, 122.8, 124.3, 124.8, 126.0, 126.2, 126.7, 127.2, 127.7, 128.9, 129.0, 130.2, 130.3, 131.6, 134.1, 136.3, 138.9, 143.1, 143.4, 165.2. HRMS (ESI) *m/z* 410.1385 $[M+H]^+$ (calcd. for $[C_{26}H_{20}NO_4]^+$ 410.1392).

4.1.34. (±) 8-(4-Fluorobenzyl)-6-naphthalen-1-yl-8H-1,3,5-trioxa-8-azacyclopenta[b]naphthalen-7-one ***(5m)***

Following the same procedure described for **5a**, and starting from **13c** (0.190 g, 0.595 mmol) and 4-fluorobenzyl bromide (0.135 g, 0.714 mmol), the title compound was obtained as white solid (0.122 g, yield 48%); mp: 134-135 °C; ^{1}H NMR (300 MHz, $CDCl_3$) δ: 5.24 (q, 2H, *J* = 16.4 Hz), 5.85 (d, 2H, *J* = 6.0 Hz), 6.32 (s, 1H), 6.42 (s, 1H), 6.59 (s, 1H), 7.08 (t, 2H, *J* = 8.5 Hz), 7.39 (m, 4H), 7.58 (qt, 2H, *J* = 7.7 Hz), 7.89 (m, 2H), 8.28 (d, 1H, *J* = 8.2 Hz); ^{13}C NMR (75 MHz, $CDCl_3$) δ: 45.3, 77.7, 97.1, 100.1, 101.5, 115.9 (d, $J_{C\text{-}F}$ = 21.6 Hz), 122.5, 124.2, 124.8, 126.1, 126.1, 126.7, 129.0, 129.1 (d, $J_{C\text{-}F}$ = 13.8 Hz), 130.2, 130.3, 131.5, 132.0 (d, $J_{C\text{-}F}$ = 3.2 Hz), 134.1, 138.9, 143.1, 143.5, 162.2 (d, $J_{C\text{-}F}$ = 246.1 Hz), 165.2. HRMS (ESI) *m/z* 428.1263 $[M+H]^+$ (calcd. for $[C_{26}H_{19}FNO_4]^+$ 428.1298).

*4.1.35. (±) 8-Methyl-6-naphthalen-1-yl-8H-1,3,5-trioxa-8-azacyclopenta[b]naphthalen-7-one (****5n****)*

Following the same procedure described for **5a**, and starting from **13c** (0.210 g, 0.658 mmol) and iodomethane (0.187 g, 1.32 mmol), the title compound was obtained as white solid (0.167 g, yield 76%); 171-173 °C; ^{1}H NMR (300 MHz, $CDCl_3$) δ: 3.52 (s, 3H), 5.89 (d, 2H, *J* = 14.3 Hz), 6.27 (s, 1H), 6.41 (s, 1H), 6.64 (s, 1H), 7.34 (m, 2H), 7.52-7.64 (m, 2H), 7.87 (t, 2H, *J* = 8.6 Hz), 8.28 (d, 1H, *J* = 8.4 Hz); ^{13}C NMR (75 MHz, $CDCl_3$) δ: 29.2, 77.4, 96.5, 100.0, 101.5, 123.6, 124.2, 124.8, 125.9, 126.0, 126.7,

128.8, 130.2, 131.6, 134.1, 138.5, 143.2, 143.3, 165.0. HRMS (ESI) *m/z* 334.1078 $[M+H]^+$ (calcd. for $[C_{20}H_{16}NO_4]^+$ 334.1079).

*4.1.36. (±) 8-Ethyl-6-naphthalen-1-yl-8H-1,3,5-trioxa-8-azacyclopenta[b]naphthalen-7-one (**5o**)*

Following the same procedure described for **5a**, and starting from **13c** (0.180 g, 0.564 mmol) and iodoethane (0.176 g, 1.13 mmol), the title compound was obtained as white solid (0.157 g, yield 80%); mp: 144-146 °C; ^{1}H NMR (300 MHz, $CDCl_3$) δ: 1.44 (t, 3H, *J* = 7.1 Hz), 4.01-4.22 (m, 2H), 5.88 (d, 2H, *J* = 16.1 Hz), 6.26 (s, 1H), 6.38 (s, 1H), 6.66 (s, 1H), 7.27-7.38 (m, 2H), 7.54-7.64 (m, 2H), 7.86 (t, 2H, *J* = 9.2 Hz), 8.30 (d, 1H, *J* = 8.3 Hz); ^{13}C NMR (75 MHz, $CDCl_3$) δ: 12.9, 37.5, 77.1, 96.3, 100.3, 101.5, 122.4, 124.2, 124.8, 125.7, 126.0, 126.7, 128.8, 130.1, 131.7, 134.1, 138.6, 143.2, 143.2, 164.3. HRMS (ESI) *m/z* 348.1235 $[M+H]^+$ (calcd. for $[C_{21}H_{18}NO_4]^+$ 348.1236).

*4.1.37. (±) 8-Benzyl-6-naphthalen-2-yl-8H-1,3,5-trioxa-8-azacyclopenta[b]naphthalen-7-one (**5p**)*

Following the same procedure described for **5a**, and starting from **13d** (0.190 g, 0.595 mmol) and benzyl bromide (0.122 g, 0.714 mmol), the title compound was obtained as white solid (0.173 g, yield 71%); mp: 130-132 °C; ^{1}H NMR (300 MHz, $CDCl_3$) δ: 5.04 (d, 1H, *J* = 16.1), 5.36 (d, 1H, *J* = 16.1 Hz), 5.85 (d, 2H, *J* = 16.0 Hz), 5.95 (s, 1H), 6.42 (s, 1H), 6.68 (s, 1H), 7.26-7.33 (m, 5H), 7.49-7.52 (m, 2H), 7.62 (d, 1H, *J* = 8.6 Hz), 7.79-7.88 (m, 4H); ^{13}C NMR (75 MHz, $CDCl_3$) δ: 45.9, 78.7, 97.3, 100.1, 101.5, 122.4, 124.3, 126.3, 126.4, 126.6, 126.6, 127.6, 127.7, 128.2, 128.6, 128.9, 132.2, 132.9, 133.3, 136.0, 138.6, 143.0, 143.6, 164.6. HRMS (ESI) *m/z* 410.1363 $[M+H]^+$ (calcd. for $[C_{26}H_{20}NO_4]^+$ 410.1392).

*4.1.38. (±) 8-Benzyl-6-phenyl-8H-1,3,5-trioxa-8-azacyclopenta[b]naphthalen-7-one (**5q**)*

Following the same procedure described for **5a**, and starting from **13e** (0.150 g, 0.557 mmol) and benzyl bromide (0.114 g, 0.669 mmol), the title compound was obtained as white solid (0.154 g, yield 77%); mp: 133-135 °C; ^{1}H NMR (300 MHz, $CDCl_3$) δ: 5.04 (d, 1H, *J* = 16.1 Hz), 5.29 (d, 1H, *J* = 16.1 Hz), 5.78 (s, 1H), 5.87 (d, 2H, *J* = 7.3 Hz), 6.42 (s, 1H), 6.64 (s, 1H), 7.22-7.48 (m, 10H); ^{13}C NMR (75 MHz,

$CDCl_3$) δ: 45.8, 78.6, 97.3, 100.0, 101.5, 122.2, 126.5, 126.8, 127.5, 128.6, 128.8, 128.9, 134.8, 135.9, 142.9, 143.5, 164.6. HRMS (ESI) *m/z* 360.1227 $[M+H]^+$ (calcd. for $[C_{22}H_{18}NO_4]^+$ 360.1236).

*4.1.39. (±) 8-Methyl-6-phenyl-8H-1,3,5-trioxa-8-azacyclopenta[b]naphthalen-7-one (**5r**)*

Following the same procedure described for **5a**, and starting from **13e** (0.140 g, 0.520 mmol) and iodomethane (0.148 g, 1.04 mmol), the title compound was obtained as white solid (0.112 g, yield 76%); 153-155 °C; ^1H NMR (300 MHz, $CDCl_3$) δ: 3.40 (s, 3H), 5.66 (s, 1H), 5.93 (d, 2H, *J* = 16.1 Hz), 6.54 (s, 1H), 6.63 (s, 1H), 7.53 (m, 5H); ^{13}C NMR (75 MHz, $CDCl_3$) δ: 29.1, 78.6, 99.6, 99.9, 101.5, 123.1, 126.9, 128.6, 128.7, 135.0, 138.5, 143.0, 143.4, 164.4. HRMS (ESI) *m/z* 284.0923 $[M+H]^+$ (calcd. for $[C_{16}H_{14}NO_4]^+$ 284.0923).

*4.1.40. (±) 8-Ethyl-6-phenyl-8H-1,3,5-trioxa-8-azacyclopenta[b]naphthalen-7-one (**5s**)*

Following the same procedure described for **5a**, and starting from **13e** (0.250 g, 0.929 mmol) and iodoethane (0.290 g, 1.86 mmol), the title compound was obtained as white solid (0.215, yield 78%); 82-84 °C; ^1H NMR (300 MHz, $CDCl_3$) δ: 1.31 (t, 3H, *J* = 7.2 Hz), 3.90-4.09 (m, 2H), 5.63 (s, 1H), 5.92 (dd, 2H, *J* = 9.1, 1.3 Hz), 6.55 (s, 1H), 6.61 (s, 1H), 7.35 (m, 5H); ^{13}C NMR (75 MHz, $CDCl_3$) δ: 12.7, 37.2, 78.46, 95.4, 100.2, 101.5, 121.8, 126.9, 128.6, 128.7, 135.0, 138.6, 143.1, 143.3, 163.8. HRMS (ESI) *m/z* 298.1079 $[M+H]^+$ (calcd. for $[C_{17}H_{16}NO_4]^+$ 298.1079).

*4.1.41. 3-(p-Tolyl)-1H-indol-2-yl acetate (**6a**)*

To a solution of compound **19a** (100 mg, 0.45 mmol) in 8 mL of dry DCM 2,6-lutidine (105 µL, 0.90 mmol) was added. Acetyl chloride (64 µL, 0.90 mmol) was then added dropwise to the solution cooled in an ice bath at 0 °C. After stirring at rt for 16 h the reaction mixture was poured into a beaker containing ice and brine (8 mL). The aqueous phase was extracted with DCM (3 x 10 mL) then the combined organic phases were dried over anhydrous Na_2SO_4, filtered and concentrated. The crude product was purified by flash chromatography on silica gel (10% diethyl ether in petroleum ether) to give a white solid (yield 10%); ^1H NMR (300 MHz, $CDCl_3$) δ: 8.95 (b, 1H), 7.78 (d, *J* = 7.0 Hz, 1H), 7.53 (d, *J* = 8.1 Hz, 2H),

7.37 – 7.05 (m, 5H), 2.42 (s, 3H), 2.34 (s, 3H); ^{13}C NMR (75 MHz, $CDCl_3$) δ: 169.0, 139.5, 136.0, 131.4, 130.1, 129.6 (2), 128.7 (2), 125.4, 122.4, 120.92, 119.6, 111.3, 101.9, 21.5, 21.4; ESI-MS *m/z* 287.9 $[M+Na]^+$; HRMS (ESI) *m/z* 288,1002 $[M+Na]^+$ (calcd. for $[C_{17}H_{15}NNaO_2]^+$ 288,0995).

*4.1.42. 3-(Naphthalen-1-yl)-1H-indol-2-yl acetate (**6b**)*

Title compound was obtained following the procedure reported for compound **6a**. The crude product was purified by flash chromatography on silica gel (20% EtOAc in *n*-hexane) to give a white solid (yield 42%); ^{1}H NMR (300 MHz, $CDCl_3$) δ: 9.04 (b, 1H), 7.99 – 7.85 (m, 3H), 7.64 – 7.58 (m, 2H), 7.54 – 7.49 (m, 1H), 7.46 – 7.36 (m, 3H), 7.27 (t, *J* = 7.6 Hz, 1H), 7.14 (t, *J* = 7.5 Hz, 1H), 2.15 (s, 3H); ^{13}C NMR (75 MHz, $CDCl_3$) δ: 169.2, 140.1, 134.3, 132.7, 131.5, 130.4, 128.7, 128.6, 127.9, 127.1, 126.8, 126.1, 126.0, 125.9, 122.5, 120.9, 120.2, 111.4, 101.0, 21.2; ESI-MS *m/z* 324 $[M+Na]^+$, 340 $[M+K]^+$; HRMS (ESI) *m/z* 324,0995 $[M+Na]^+$ (calcd. for $[C_{20}H_{15}NNaO_2]^+$ 324,0995)

*4.1.43. 3-(Naphthalen-1-yl)-1H-indol-2-yl diethylcarbamate (**6c**)*

Title compound was obtained, following the procedure reported for compound **6a**, starting from **19b** (100 mg, 0.39 mmol) and using diethylcarbamoyl chloride (149 μL, 1.17 mmol). The crude product was purified by flash chromatography on silica gel (17% EtOAc in *n*-hexane) to give a white solid (yield 30%); ^{1}H NMR (300 MHz, $CDCl_3$) δ: 9.50 (s, 1H), 8.01 – 7.84 (m, 3H), 7.67 – 7.35 (m, 6H), 7.27 – 7.17 (m, 1H), 7.15 – 7.06 (m, 1H), 3.31 (q, *J* = 7.2 Hz, 2H), 3.01 (q, *J* = 14.3, 7.2 Hz, 2H), 1.14 (t, *J* = 7.1 Hz, 3H), 0.75 (t, *J* = 7.1 Hz, 3H); ^{13}C NMR (75 MHz, $CDCl_3$) δ: 153.0, 141.4, 134.3, 132.7, 131.6, 130.9, 128.6, 128.4, 127.4, 127.1, 127.0, 125.9, 125.8, 125.7, 121.8, 120.6, 119.6, 111.3, 99.5, 42.7, 42.4, 13.8, 13.4; ESI-MS *m/z* 359.0 $[M+H]^+$, 381.0 $[M+Na]^+$; HRMS (ESI) *m/z* 359,1762 $[M+H]^+$ (calcd. for $[C_{23}H_{23}N_2O_2]^+$ 359,1754).

4.2. Computational studies

4.2.1. Ligands preparation

Compounds were built using Maestro (Maestro version 9.2, Schrödinger, LLC, New York, NY, 2011). Energy minimizations were performed by means of MacroModel (MacroModel version 9.9, Schrödinger, LLC, New York, NY, 2011) using the OPLS-AA 2005 as force field [53, 54]. The solvent effects are simulated adopting the analytical Generalized-Born/Surface-Area (GB/SA) model [55], and no cutoff for nonbonded interactions was employed. Polak-Ribiere conjugate gradient (PRCG) technique with 1,000 maximum iterations and 0.001 gradient convergence threshold was used. Moreover, compounds were submitted to LigPrep application (LigPrep version 9.2, Schrödinger, LLC, New York, NY, 2011) in order to generate the most probable ionization state at cellular pH value (7.4 ± 0.2) as reported by us [56, 57].

4.2.2. Protein Preparation

The three-dimensional structures of the *h*AK and *h*GSK-3β enzymes were taken from PDB (entry 1BX4 and 1H8F, respectively). The proteins were imported into Schrödinger Maestro molecular modeling environment. Water molecules, ions were removed and the resulting structures were submitted to protein preparation wizard workflow available in Maestro suite 2011. By using this protocol, we obtained a reasonable starting structure of proteins for molecular docking calculations. In particular the protocol included three steps to: (1) add hydrogen atoms, (2) optimize the orientation of hydroxyl groups, Asn, and Gln, and the protonation state of His, and (3) perform a constrained refinement by employing impref application (max RMSD = 0.30). The latter consists of a cycles of energy minimization based on the impact molecular mechanics engine and on the OPLS_2005 force field [58, 59].

4.2.3. Molecular docking

4.2.3.1. Induced Fit Docking

Molecular docking was carried out using the Schrödinger suite 2011 by applying the IFD protocol. This procedure induces conformational changes in the binding site to accommodate the ligand and exhaustively identify possible binding modes and associated conformational changes by side-chain sampling and backbone minimization. The proteins and the ligands were prepared as reported in the

previous paragraphs. The boxes for docking calculation were built from the center of the gorge selecting the residues F338 in *h*AK and R209 in *h*GSK-3β with default setting. IFD includes protein side-chain flexibility in a radius of 5.0 Å around the poses found during the early docking stage of the IFD protocol. Complexes within 30.0 kcal/mol of minimum energy structure were taken forward for redocking. The Glide redocking stage was performed by XP (Extra Precision) methods. The calculations were performed using default IFD protocol parameters. No constraints were used.

4.2.3.2. Blind docking

Computational investigation by means of blind docking technique was carried out by using AutoDock employing the Graphical User Interface program AutoDockTools 4.2 (ADT 4.2) [51, 60]. The protein (*h*AK) and both enantiomers of ligand (**5l**) were prepared by means of ADT for generating the structure files for AutoDock in .pdbqt format. ADT assigned polar hydrogens, Kollman charges, fragmental volumes and solvation parameters to the protein. AutoGrid software was employed for preparing the grid map using a grid box. The grid size was set to 86 x 45 x 69 xyz points with grid spacing of 1 Å and the grid center was selected at dimensions (x, y, and z): 47.3 x 16.2 x 38.4. By adopting these parameters the whole protein was considered for the blind docking investigation. During the docking calculation the enzyme was considered as rigid. Docking calculations of **5l** were performed employing the Lamarckian genetic algorithm (GA) and through a protocol with an initial population of 150 randomly placed individuals, a maximum number of 2,5 million energy evaluations. For the local search a maximum of 500 GA runs was considered. The docked solutions for the (*R*)-enantiomer comprised between -7.76 kcal/mol and -5.88 kcal/mol corresponding to an estimated affinity range of 2.06-50 μM (Figure 4A). While, for the (*S*)-enantiomer, the docked solutions comprised between -7.93 kcal/mol and -5.85 kcal/mol corresponding to an estimated affinity range of 1.55-50 μM (Figure 4B).

4.3. Biological evaluation

4.3.1. Enzymes inhibition assays

4.3.1.1. Materials

For biological tests analytical grade reagents were exclusively used. His-tagged *h*GSK-3β was purchased by Sigma-Aldrich (cat. n° G4296). His-tagged *h*AK was expressed and purified as previously described [43], [^{33}P]γ-ATP, 3000 Ci/mmol (10 mCi/mL), and [2,8-^{3}H]-Adenosine, 29.1 Ci/mmol (1 mCi/mL) were from Hartmann Analytics (Germany). Phospho-Glycogen Synthase Peptide-2 (GS-2), YRRAAVPPSPSLSRHSSPHQ(pS)EDEEE, was purchased from Millipore (cat. n° 12-241).

4.3.1.2. Human GSK-3β activity assay

GSK-3β kinase activity was measured, in the presence or absence of the putative inhibitors, as described by the supplier, Sigma-Aldrich. Briefly, *h*GSK-3β (2.5 ng) was assayed in a reaction mixture (25 µl) containing final concentrations of: 10 mM MOPS pH 7.2; 0.2 mM EDTA; 0.5 mM EGTA, 2 mM $MgCl_2$; 0.25 mM DTT; 50 ng/µl BSA, 1% (v/v) DMSO, 10 µM [^{33}P]γ-ATP (75 Ci/mmol) and 13 µM GS-2 peptide substrate. The GS-2 peptide sequence is similar to skeletal muscle glycogen synthase. Following 15 min incubation at 30 °C, the reaction was stopped by spotting 10 µl of the incubated mixture onto P30 96-square glass fiber filter (Filtermat, Wallac). The filter was rinsed three times (10 min each) in 0.43% phosphoric acid solution, in order to remove unreacted [^{33}P]-ATP and finally in aceton. The filter was dried, melt-on scintillator sheets (MeltiLex A, Perkin Elmer) and labeled GS-2 peptide trapped on filter was quantified by Microbeta Trilux (Perkin Elmer) luminometer, according to the manufacturer's protocol.

When putative inhibitors were evaluated, five concentrations of each compound (dissolved at 10 mM in 100% DMSO) were tested in triplicate, at 1% final DMSO concentration in the assay. DMSO at 1% had no effect on *h*GSK-3β activity (data not shown).

4.3.1.3 Human AK activity assay

*h*AK was assayed in 15 µL of a mixture containing 64 mM Tris-HCl pH 7.5, 40 mM KCl, 0.1 mM $MgCl_2$, 0.1 mM ATP, and 1 µM [2,8-^{3}H]-Adenosine. After 20 min at 37 °C the reaction was stopped by spotting 10 µL of the incubated mixture onto DEAE 96-square glass fiber filter (DEAE Filtermat, Wallac). The filter was rinsed three times (5 min each) in 1 mM ammonium formate, pH 3.6, in order to remove unconverted nucleoside, and finally in ethanol. The filter was dried and radioactivity counted as above described.

When putative inhibitors were evaluated, five concentrations of each compound (dissolved at 10 mM in 100% DMSO) were tested in triplicate, at 1% final DMSO concentration in the assay. DMSO at 1% had no effect on *h*AK activity (data not shown).

4.3.2. Cytotoxicity and antioxidant evaluation

4.3.2.1. Cells preparation and neuronal differentiation

To better establish the optimal density to grow IMR 32 cells, we have seeded IMR 32 in 96-wells plate at different density: 10,000; 15,000; 20,000; 50,000; 100,000; 200,000 cells/well.

Regarding the neuronal differentiation, IMR 32 cells were seeded at the density of 25,000 cells/well in 96-wells plate and treated every two days with EMEM medium supplemented with 10% fetal bovine serum and with BrdU 10 µM. After 12 days BrdU treatment results in neurite extension as visible in Figure S8.

4.3.2.2. Cells treatments

The different formulations (**4**, **5c**,**l** and **6b**) were dissolved in DMSO as stock solutions at the final concentration of 10 mM. Stock solutions were then diluted with cell culture medium, EMEM with Earle's Balanced Salt Solution, in order to obtain an intermediate dose solution (100 µM), which was used for the serial dilution as follows: 50 µM, 10 µM, 5 µM, 1 µM, 0.5 µM and 0.1 µM for each substance. Control vehicle was represented by DMSO ranging from 0.5% to 0.001%.

4.3.2.3. Cytotoxicity determination

As mentioned above, IMR 32 cells were seeded 100,000 cells/well in 96-wells plate and were grown to confluence, then were treated with the mentioned substances in EMEM medium supplemented with 10% fetal bovine serum. The effects on cellular morphology were checked after 24 h as shown in Figure S5. Cytotoxicity was determined by LDH release in the media, measured by enzymatic assay: in the first step NAD^+ is reduced to $NADH/H^+$ by LDH-catalyzed conversion of lactate to pyruvate; in the second step the catalyst (diaphorase) transfers H/H^+ from $NADH/H^+$ to tetrazolium salt which is reduced to formazan. For total release of intracellular LDH (positive control of 100% cell death), IMR 32 were treated with 1% Triton X-100, according to the manufacturer's instructions. The amount of LDH in the supernatant was determined and calculated according to kit instructions. The amount of LDH release in each sample was determined by measuring the absorbance at 490 nm using a microplate spectrophotometer. All tests were performed at least in triplicate. The absorbance measured from three wells was averaged, and the percentage of LDH released was calculated as arbitrary unit of change relative to 1% Triton X-100 treated cells.

4.3.2.4. DCFDA determination

IMR 32 cells were seeded 100,000 cells/well in 96- wells plate and were grown to confluence, then were treated with the substances of interest in EMEM medium supplemented with 10% fetal bovine serum. After 24 h from the seeding cells were treated for 24 h with the 4 different compounds (**4, 5c,l** and **6**) at the 3 chosen doses (0,1 μM; 0,5 μM; 1 μM). Then, after 24 h from the treatment, IMR 32 cells were incubated with 5 μM DCF per 30 min; then washed two times and treated with H_2O_2 at the concentration of 50 μM for 1 h.

For neuronal differentiation, IMR 32 cells were seeded 25,000 cells/well in 96-wells plate and treated for 12 days with BrdU. After 12 days from the seeding, the resulting neuronal cells were treated for 24 h with the 4 different compounds (**4, 5c,l** and **6**) at the 3 chosen doses (0,1 μM; 0,5 μM; 1 μM). Then,

neuronal cells were incubated with 5 μM DCF for 30 min, washed two times with PBS and treated with 50 μM H_2O_2 for 1 h.

After H_2O_2 treatment, ROS levels were detected by measuring the DCF fluorescence at 495 nm and 529 nm using a microplate reader. All tests were performed at least in triplicate. The fluorescence measured from three wells was averaged, and the percentage of DCF into the cells was calculated as arbitrary unit of change relative to untreated cells. The determination was carried out in the same manner for both undifferentiated and neuronal cells.

Acknowledgements

This work was partially supported by the Consiglio Nazionale delle Ricerche/Ministro dell'Istruzione, dell'Università e della Ricerca (CNR/MIUR) "Progetto d'interesse invecchiamento" (to G.B.). L.S. was supported by a fellowship provided by CNR/MIUR "Progetto d'interesse invecchiamento". The British Society for Antimicrobial Chemotherapy (BSAC) is kindly acknowledged (grant number GA2016_087R to Si.Br.).

Appendix A. Supplementary data

Supplementary data associated to this article (Figures S1-S8 and HMBC experiments for compounds **5a-d,f**) can be found at….

References

[1] H. Sies, Oxidative stress: a concept in redox biology and medicine, Redox Biol, 4 (2015) 180-183.
[2] C. Cervellati, P.L. Wood, A. Romani, G. Valacchi, M. Squerzanti, J.M. Sanz, B. Ortolani, G. Zuliani, Oxidative challenge in Alzheimer's disease: state of knowledge and future needs, J Investig Med, 64 (2016) 21-32.
[3] S. Dhib-Jalbut, D.L. Arnold, D.W. Cleveland, M. Fisher, R.M. Friedlander, M.M. Mouradian, S. Przedborski, B.D. Trapp, T. Wyss-Coray, V.W. Yong, Neurodegeneration and neuroprotection in multiple sclerosis and other neurodegenerative diseases, J Neuroimmunol, 176 (2006) 198-215.
[4] J.T. Coyle, P. Puttfarcken, Oxidative stress, glutamate, and neurodegenerative disorders, Science, 262 (1993) 689-695.
[5] G.H. Kim, J.E. Kim, S.J. Rhie, S. Yoon, The Role of Oxidative Stress in Neurodegenerative Diseases, Exp Neurobiol, 24 (2015) 325-340.
[6] G.C. Higgins, P.M. Beart, Y.S. Shin, M.J. Chen, N.S. Cheung, P. Nagley, Oxidative stress: emerging mitochondrial and cellular themes and variations in neuronal injury, J Alzheimers Dis, 20 Suppl 2 (2010) S453-473.
[7] J.K. Andersen, Oxidative stress in neurodegeneration: cause or consequence?, Nat Med, 10 Suppl (2004) S18-25.
[8] Y. Liu, D.R. Schubert, The specificity of neuroprotection by antioxidants, J Biomed Sci, 16 (2009) 98.
[9] K.K. Jain, Handbook of Neuroprotection, Springer Science+Business Media, Switzerland, 2011, (2011) 1-547.
[10] B. Carletti, F. Piemonte, F. Rossi, Neuroprotection: the emerging concept of restorative neural stem cell biology for the treatment of neurodegenerative diseases, Curr Neuropharmacol, 9 (2011) 313-317.
[11] S. Brogi, S. Butini, S. Maramai, R. Colombo, L. Verga, C. Lanni, E. De Lorenzi, S. Lamponi, M. Andreassi, M. Bartolini, V. Andrisano, E. Novellino, G. Campiani, M. Brindisi, S. Gemma, Disease-modifying anti-Alzheimer's drugs: inhibitors of human cholinesterases interfering with beta-amyloid aggregation, CNS Neurosci Ther, 20 (2014) 624-632.
[12] M.L. Bolognesi, A. Cavalli, L. Valgimigli, M. Bartolini, M. Rosini, V. Andrisano, M. Recanatini, C. Melchiorre, Multi-target-directed drug design strategy: from a dual binding site acetylcholinesterase inhibitor to a trifunctional compound against Alzheimer's disease, J Med Chem, 50 (2007) 6446-6449.
[13] L. Ismaili, B. Refouvelet, M. Benchekroun, S. Brogi, M. Brindisi, S. Gemma, G. Campiani, S. Filipic, D. Agbaba, G. Esteban, M. Unzeta, K. Nikolic, S. Butini, J. Marco-Contelles, Multitarget compounds bearing tacrine- and donepezil-like structural and functional motifs for the potential treatment of Alzheimer's disease, Prog Neurobiol, (2016) doi: 10.1016/j.pneurobio.2015.1012.1003.
[14] S. Butini, K. Nikolic, S. Kassel, H. Bruckmann, S. Filipic, D. Agbaba, S. Gemma, S. Brogi, M. Brindisi, G. Campiani, H. Stark, Polypharmacology of dopamine receptor ligands, Prog Neurobiol, 142 (2016) 68-103.
[15] L.M. Espinoza-Fonseca, The benefits of the multi-target approach in drug design and discovery, Bioorg Med Chem, 14 (2006) 896-897.
[16] B. Martin, R.L. de Maturana, R. Brenneman, T. Walent, M.P. Mattson, S. Maudsley, Class II G protein-coupled receptors and their ligands in neuronal function and protection, Neuromolecular Med, 7 (2005) 3-36.
[17] V.A. Doze, D.M. Perez, G-Protein-Coupled Receptors in Adult Neurogenesis, Pharmacol Rev, 64 (2012) 645-675.
[18] F. Prati, A. De Simone, A. Armirotti, M. Surnma, D. Pizzirani, R. Scarpelli, S.M. Bertozzi, D.I. Perez, V. Andrisano, A. Perez-Castillo, B. Monti, F. Massenzio, L. Polito, M. Racchi, P. Sabatino, G. Bottegoni, A. Martinez, A. Cavalli, M.L. Bolognesi, 3,4-Dihydro-1,3,5-triazin-2(1H)-ones as the First Dual BACE-1/GSK-3 beta Fragment Hits against Alzheimer's Disease, ACS Chem Neurosci, 6 (2015) 1665-1682.
[19] D.P. Singh, K. Chopra, Flavocoxid, dual inhibitor of cyclooxygenase-2 and 5-lipoxygenase, exhibits neuroprotection in rat model of ischaemic stroke, Pharmacol Biochem Behav, 120 (2014) 33-42.
[20] K.H. Jeon, E. Lee, K.Y. Jun, J.E. Eom, S.Y. Kwak, Y. Na, Y. Kwon, Neuroprotective effect of synthetic chalcone derivatives as competitive dual inhibitors against mu-calpain and cathepsin B through the downregulation of tau phosphorylation and insoluble A beta peptide formation, Eur J Med Chem, 121 (2016) 433-444.

[21] V. Naidoo, D.A. Karanian, S.K. Vadivel, J.R. Locklear, J.T. Wood, M. Nasr, P.M. Quizon, E.E. Graves, V. Shukla, A. Makriyannis, B.A. Bahr, Equipotent inhibition of fatty acid amide hydrolase and monoacylglycerol lipase - dual targets of the endocannabinoid system to protect against seizure pathology, Neurotherapeutics, 9 (2012) 801-813.
[22] M. Brindisi, S. Brogi, S. Maramai, A. Grillo, G. Borrelli, S. Butini, E. Novellino, M. Allara, A. Ligresti, G. Campiani, V. Di Marzo, S. Gemma, Harnessing the pyrroloquinoxaline scaffold for FAAH and MAGL interaction: definition of the structural determinants for enzyme inhibition, RSC Adv, 6 (2016) 64651-64664.
[23] S. Butini, S. Gemma, G. Campiani, S. Franceschini, F. Trotta, M. Borriello, N. Ceres, S. Ros, S.S. Coccone, M. Bernetti, M. De Angelis, M. Brindisi, V. Nacci, I. Fiorini, E. Novellino, A. Cagnotto, T. Mennini, K. Sandager-Nielsen, J.T. Andreasen, J. Scheel-Kruger, J.D. Mikkelsen, C. Fattorusso, Discovery of a New Class of Potential Multifunctional Atypical Antipsychotic Agents Targeting Dopamine D-3 and Serotonin 5-HT1A and 5-HT2A Receptors: Design, Synthesis, and Effects on Behavior, J Med Chem, 52 (2009) 151-169.
[24] M. Brindisi, S. Butini, S. Franceschini, S. Brogi, F. Trotta, S. Ros, A. Cagnotto, M. Salmona, A. Casagni, M. Andreassi, S. Saponara, B. Gorelli, P. Weikop, J.D. Mikkelsen, J. Scheel-Kruger, K. Sandager-Nielsen, E. Novellino, G. Campiani, S. Gemma, Targeting Dopamine D-3 and Serotonin 5-HT1A and 5-HT2A Receptors for Developing Effective Antipsychotics: Synthesis, Biological Characterization, and Behavioral Studies, J Med Chem, 57 (2014) 9578-9597.
[25] S. Maramai, S. Gemma, S. Brogi, G. Campiani, S. Butini, H. Stark, M. Brindisi, Dopamine D3 Receptor Antagonists as Potential Therapeutics for the Treatment of Neurological Diseases, Front Neurosci, 10 (2016) 451.
[26] S. Butini, G. Campiani, M. Borriello, S. Gemma, A. Panico, M. Persico, B. Catalanotti, S. Ros, M. Brindisi, M. Agnusdei, I. Fiorini, V. Nacci, E. Novellino, T. Belinskaya, A. Saxena, C. Fattorusso, Exploiting protein fluctuations at the active-site gorge of human cholinesterases: Further optimization of the design strategy to develop extremely potent inhibitors, J Med Chem, 51 (2008) 3154-3170.
[27] M.Y. Wu, G. Esteban, S. Brogi, M. Shionoya, L. Wang, G. Campiani, M. Unzeta, T. Inokuchi, S. Butini, J. Marco-Contelles, Donepezil-like multifunctional agents: Design, synthesis, molecular modeling and biological evaluation, Eur J Med Chem, 121 (2016) 864-879.
[28] M. Chioua, M. Perez, O.M. Bautista-Aguilera, M. Yanez, M.G. Lopez, A. Romero, R. Cacabelos, R.P. de la Bellacasa, S. Brogi, S. Butini, J.I. Borrell, J. Marco-Contelles, Development of HuperTacrines as non-toxic, cholinesterase inhibitors for the potential treatment of Alzheimer's disease, Mini Rev Med Chem, 15 (2015) 648-658.
[29] S. Butini, M. Brindisi, S. Brogi, S. Maramai, E. Guarino, A. Panico, A. Saxena, V. Chauhan, R. Colombo, L. Verga, E. De Lorenzi, M. Bartolini, V. Andrisano, E. Novellino, G. Campiani, S. Gemma, Multifunctional cholinesterase and amyloid Beta fibrillization modulators. Synthesis and biological investigation, ACS Med Chem Lett, 4 (2013) 1178-1182.
[30] L. Zaccagnini, S. Brogi, M. Brindisi, S. Gemma, G. Chemi, G. Legname, G. Campiani, S. Butini, Identification of novel fluorescent probes preventing PrPSc replication in prion diseases, Eur J Med Chem, 127 (2017) 859-873.
[31] M.K. Pandey, T.R. DeGrado, Glycogen Synthase Kinase-3 (GSK-3)-Targeted Therapy and Imaging, Theranostics, 6 (2016) 571-593.
[32] C. Hooper, R. Killick, S. Lovestone, The GSK3 hypothesis of Alzheimer's disease, J Neurochem, 104 (2008) 1433-1439.
[33] C.S. Kuruva, P.H. Reddy, Amyloid beta modulators and neuroprotection in Alzheimer's disease: a critical appraisal, Drug Discov Today, 22 (2017) 223-233.
[34] M. Golpich, E. Amini, F. Hemmati, N.M. Ibrahim, B. Rahmani, Z. Mohamed, A.A. Raymond, L. Dargahi, R. Ghasemi, A. Ahmadiani, Glycogen synthase kinase-3 beta (GSK-3beta) signaling: Implications for Parkinson's disease, Pharmacol Res, 97 (2015) 16-26.
[35] M. Schafer, S. Goodenough, B. Moosmann, C. Behl, Inhibition of glycogen synthase kinase 3 beta is involved in the resistance to oxidative stress in neuronal HT22 cells, Brain Research, 1005 (2004) 84-89.
[36] K.Y. Lee, S.H. Koh, M.Y. Noh, K.W. Park, Y.J. Lee, S.H. Kim, Glycogen synthase kinase-3beta activity plays very important roles in determining the fate of oxidative stress-inflicted neuronal cells, Brain Research, 1129 (2007) 89-99.

[37] G. Pignataro, R.P. Simon, D. Boison, Transgenic overexpression of adenosine kinase aggravates cell death in ischemia, J Cereb Blood Flow Metab, 27 (2007) 1-5.
[38] G. Pignataro, S. Maysami, F.E. Studer, A. Wilz, R.P. Simon, D. Boison, Downregulation of hippocampal adenosine kinase after focal ischemia as potential endogenous neuroprotective mechanism, J Cereb Blood Flow Metab, 28 (2008) 17-23.
[39] V. Ramkumar, K.A. Jhaveri, X. Xie, S. Jajoo, L.A. Toth, Nuclear Factor kappaB and Adenosine Receptors: Biochemical and Behavioral Profiling, Curr Neuropharmacol, 9 (2011) 342-349.
[40] D. Boison, Adenosine kinase: exploitation for therapeutic gain, Pharmacol Rev, 65 (2013) 906-943.
[41] D. Boison, J.F. Chen, B.B. Fredholm, Adenosine signaling and function in glial cells, Cell Death Differ, 17 (2010) 1071-1082.
[42] L. Savi, M. Brindisi, G. Alfano, S. Butini, V. La Pietra, E. Novellino, L. Marinelli, A. Lossani, F. Focher, C. Cavella, G. Campiani, S. Gemma, Site-directed Mutagenesis of Key Residues Unveiled a Novel Allosteric Site on Human Adenosine Kinase for Pyrrolobenzoxa(thia)zepinone Non-Nucleoside Inhibitors, Chem Biol Drug Des, 87 (2016) 112-120.
[43] S. Butini, S. Gemma, M. Brindisi, G. Borrelli, A. Lossani, A.M. Ponte, A. Torti, G. Maga, L. Marinelli, V. La Pietra, I. Fiorini, S. Lamponi, G. Campiani, D.M. Zisterer, S.M. Nathwani, S. Sartini, C. La Motta, F. Da Settimo, E. Novellino, F. Focher, Non-nucleoside inhibitors of human adenosine kinase: synthesis, molecular modeling, and biological studies, J Med Chem, 54 (2011) 1401-1420.
[44] H. Eldar-Finkelman, A. Martinez, GSK-3 Inhibitors: Preclinical and Clinical Focus on CNS, Front Mol Neurosci, 4 (2011) 32.
[45] V. Palomo, I. Soteras, D.I. Perez, C. Perez, C. Gil, N.E. Campillo, A. Martinez, Exploring the binding sites of glycogen synthase kinase 3. Identification and characterization of allosteric modulation cavities, J Med Chem, 54 (2011) 8461-8470.
[46] J. Bain, L. Plater, M. Elliott, N. Shpiro, C.J. Hastie, H. McLauchlan, I. Klevernic, J.S. Arthur, D.R. Alessi, P. Cohen, The selectivity of protein kinase inhibitors: a further update, Biochem J, 408 (2007) 297-315.
[47] P. Zhang, S. Li, Y. Gao, W. Lu, K. Huang, D. Ye, X. Li, Y. Chu, Novel benzothiazinones (BTOs) as allosteric modulator or substrate competitive inhibitor of glycogen synthase kinase 3beta (GSK-3beta) with cellular activity of promoting glucose uptake, Bioorg Med Chem Lett, 24 (2014) 5639-5643.
[48] M.M. Mc Gee, S. Gemma, S. Butini, A. Ramunno, D.M. Zisterer, C. Fattorusso, B. Catalanotti, G. Kukreja, I. Fiorini, C. Pisano, C. Cucco, E. Novellino, V. Nacci, D.C. Williams, G. Campiani, Pyrrolo[1,5]benzoxa(thia)zepines as a new class of potent apoptotic agents. Biological studies and identification of an intracellular location of their drug target, J Med Chem, 48 (2005) 4367-4377.
[49] Z.K. Ying, R. Desikan, X.H. Xu, A. Maiseyeu, C.Q. Liu, Q.H. Sun, O. Ziouzenkova, S. Parthasarathy, S. Rajagopalan, Modified methylenedioxyphenol analogs lower LDL cholesterol through induction of LDL receptor expression, J Lipid Res, 53 (2012) 879-887.
[50] K.D. Rynearson, B. Charrette, C. Gabriel, J. Moreno, M.A. Boerneke, S.M. Dibrov, T. Hermann, 2-Aminobenzoxazole ligands of the hepatitis C virus internal ribosome entry site, Bioorg Med Chem Lett, 24 (2014) 3521-3525.
[51] G.M. Morris, R. Huey, W. Lindstrom, M.F. Sanner, R.K. Belew, D.S. Goodsell, A.J. Olson, AutoDock4 and AutoDockTools4: Automated docking with selective receptor flexibility, J Comput Chem, 30 (2009) 2785-2791.
[52] M. Brindisi, C. Cavella, S. Brogi, A. Nebbioso, J. Senger, S. Maramai, A. Ciotta, C. Iside, S. Butini, S. Lamponi, E. Novellino, L. Altucci, M. Jung, G. Campiani, S. Gemma, Phenylpyrrole-based HDAC inhibitors: synthesis, molecular modeling and biological studies, Future Med Chem, 8 (2016) 1573-1587.
[53] W.L. Jorgensen, D.S. Maxwell, J. TiradoRives, Development and testing of the OPLS all atom force field on conformational energetics and properties of organic liquids J. Am. Chem. Soc., 118 (1996) 11225-11236.
[54] G.A. Kaminski, R.A. Friesner, J. Tirado-Rives, W.L. Jorgensen, Evaluation and reparametrization of the OPLS-AA force field for proteins via comparison with accurate quantum chemical calculations on peptides, J. Phys. Chem. B, 105 (2001) 6474-6487.
[55] W.C. Still, A. Tempczyk, R.C. Hawley, T. Hendrickson, Semianalytical Treatment of Solvation for Molecular Mechanics and Dynamics, J. Am. Chem. Soc., 112 (1990) 6127-6129.

[56] M. Brindisi, S. Gemma, S. Kunjir, L. Di Cerbo, S. Brogi, S. Parapini, S. D'Alessandro, D. Taramelli, A. Habluetzel, S. Tapanelli, S. Lamponi, E. Novellino, G. Campiani, S. Butini, Synthetic spirocyclic endoperoxides: new antimalarial scaffolds, Medchemcomm, 6 (2015) 357-362.
[57] S. Giovani, M. Penzo, S. Brogi, M. Brindisi, S. Gemma, E. Novellino, L. Savini, M.J. Blackman, G. Campiani, S. Butini, Rational design of the first difluorostatone-based PfSUB1 inhibitors, Bioorg Med Chem Lett, 24 (2014) 3582-3586.
[58] M. Brindisi, S. Brogi, N. Relitti, A. Vallone, S. Butini, S. Gemma, E. Novellino, G. Colotti, G. Angiulli, F. Di Chiaro, A. Fiorillo, A. Ilari, G. Campiani, Structure-based discovery of the first non-covalent inhibitors of Leishmania major tryparedoxin peroxidase by high throughput docking, Sci Rep, 5 (2015) 9705.
[59] A. Gasser, S. Brogi, K. Urayama, T. Nishi, H. Kurose, A. Tafi, N. Ribeiro, L. Desaubry, C.G. Nebigil, Discovery and cardioprotective effects of the first non-Peptide agonists of the G protein-coupled prokineticin receptor-1, Plos One, 10 (2015) e0121027.
[60] M. Brindisi, S. Maramai, S. Brogi, E. Fanigliulo, S. Butini, E. Guarino, A. Casagni, S. Lamponi, C. Bonechi, S.M. Nathwani, F. Finetti, F. Ragonese, P. Arcidiacono, P. Campiglia, S. Valenti, E. Novellino, R. Spaccapelo, L. Morbidelli, D.M. Zisterer, C.D. Williams, A. Donati, C. Baldari, G. Campiani, C. Ulivieri, S. Gemma, Development of novel cyclic peptides as pro-apoptotic agents, Eur J Med Chem, 117 (2016) 301-320.